Highly ordered mesoporous and hierarchically nanostructured meso-macroporous materials for nanotechnology, biotechnology, information technology and medical applications

Léonard, Alexandre; Vantomme, Aurélien; Bouvy, Claire; Moniotte, Nicolas; Mariaulle, Pascal; Su, Bao Lian

Published in:
Nanopages, An Interdisciplinary Journal of Nano Science and Technology

Publication date:
2006

Document Version
Early version, also known as pre-print

Nanopages 1 (2006) 1, 1–44
DOI: 10.1556/Nano.1.2006.1.1

Highly Ordered Mesoporous and Hierarchically Nanostructured Meso-macroporous Materials for Nanotechnology, Biotechnology, Information Technology and Medical Applications

Alexandre Léonard, Aurélien Vantomme, Claire Bouvy, Nicolas Moniotte, Pascal Mariaulle and Bao-Lian Su*

Laboratoire de Chimie des Matériaux Inorganiques, The University of Namur (FUNDP), 61 rue de Bruxelles, B-5000 Namur, Belgium

Abstract: A great deal of progress has recently been made in the field of ordered porous materials with uniform channel dimensions that can be adjusted over a wide range of length scales. The present paper describes the state of the art and the evolution from highly ordered mesoporous silica, aluminosilicate and pure carbon materials to our very recent success in hierarchically structured meso-macroporous carbon materials, single and binary oxides and aluminosilicates. By means of selected examples, we want to shed some light on the current strategies for the conception of these sophisticated materials. The great potential applications of these new nanomaterials emerge while their real utilisation in some expected and traditional industrial processes such as catalysis, separation, electrode materials for fuel cells and biomaterials still faces some important challenges, for example, the high price, the pelletisation and the stability (thermal, hydrothermal and water resistance). Some new perspectives, which can open the concrete applications of these materials in nanotechnology, biotechnology, information technology and medical purposes, will be prospected.

Keywords: mesoporous, meso-macroporosus, metal oxides, metallo(photo)silicates, carbons, synthesis, applications

1. Introduction

The development of our society, the conservation of our nature, the improvement of our human life and the progress in industrial technology depend on new concepts, new design and new materials. We have

* Corresponding author. Tel: 32 81 72 45 31, Fax: 32 81 72 54 14,
Email: bao-lian.su@fundp.ac.be

witnessed the great evolution and changes brought by the concept and the appearance of transistors in 1947 and silicium semiconductors in 1959 and then their immediate applications in electronic industry. The impact continuously receives its fruits. The miniaturisation goes thus from microscale to nanoscale. The question can then arise as to which scale finally we can attain? We also remember that the utilisation in some chemical processes of synthetic zeolites, a family of microporous crystalline materials, at the beginning of 1960's, just ten years after their successful synthesis in laboratory, has induced a deep revolution in petroleum refinery and petrochemical industry. This revolution has strongly marked our modern society. The materials have changed and continuously change our life. We are convinced that "No Materials, No Progress".

Facing the important global warming, the exhaustion of crude materials and oil, the strong risk of a worldwide propagation of diverse diseases (pandemic) and the super-consumption of energy, new materials with advanced properties and performant multi-functionality can be once again the driving force and the motor to find some issues of these important challenges of our modern society and human life. The recent and constant sharp increase in the price of crude oil puts materials scientists in the first front of these problems to find solutions to this new petroleum crisis, for example, new energy sources or methods for the sharp reduction of energy consumption.

Porous materials have attracted and still attract great research interest, which made a great impact in applications including catalysis, sorption, and separations [1, 2]. Major breakthroughs in porous materials synthesis since last 20 years, such as the single molecule templated synthesis of microporous molecular sieves (pore size below 2 nm), the supramolecule (surfactant assemblies) templated synthesis of mesoporous molecular sieves (pore size 2–50 nm) and latex spheres templated synthesis of macroporous materials (pore size exceeding 50 nm) have opened new fields for designing new class of nanostructured materials [3–10].

Many efforts have been devoted to the synthesis, characterisation and applications of the uniform mesoporous materials over the last decade, due to their attractive textural and structural features, e.g. highly ordered structures, ultrahigh surface areas and narrow pore size distributions in the mesopore range, tuneable pore sizes and pore structures. Progress has been made in structural, compositional, and morphological control and the stability of mesoporous materials for their emerging applications in catalysis, adsorption, sensors and biotechnologies. The demand for applications in the encapsulation and separation of proteins, where biomolecules

with large molecular weights are involved, drove the achievement of ordered mesoporous silicas with very large pore sizes near 30 nm [6, 11].

The development of modern and environmental friendly industrial processes with the highest efficiency and the lowest energy and brut materials consumption requires the more advanced and sophisticated materials having hierarchical pore structures at different length scales in order to achieve highly organized functions.

The incorporation of ordered macropores in the mesoporous materials may be somewhat more interesting and useful for catalysis and for engineering of pore systems, in comparison with bimodal mesopore size distributions. From a viewpoint of applications, for instance in catalysis, the active sites are often located in the micropores and mesopores, while the macropores favour mass transfer and reduce transport limitations. This becomes particularly important for large molecules (e.g. polymers, biomolecules) or in viscous systems, where diffusion rates are low. FCC catalysts are the concrete example of hierarchical structures in use in industry and involve the formation of a composite principally from a main component, an USY zeolite mixed with a macroporous matrix, usually amorphous silica, alumina or silica/alumina with clay. A pre-cracking of the heavy feedstocks prior to the action of the USY zeolite is carried out in macroporous matrix. The microporous openings of zeolites impede however the diffusion of bulky molecules from vacuum gas–oil and residues. The introduction of mesoporosity in USY zeolite by vapour steaming treatment can facilitate thus the secondary catalytic cracking. Finally, the more oriented cracking and the fine rearrangement of cracked molecules take place in the supercages of USY zeolite. However, this micro–meso–macroporous hierarchy was obtained by artificial mixture of different components containning predefined porosities. For the sake of large performance improvement, such materials should possess adjustable and well-defined macropores and tuneable, interconnected mesopore types of different sizes inside the macropore walls. On all length scales, the larger pores should be connected through the smaller pores. Thus, it remains a challenge to fabricate the hierarchically bimodal mesoporous-macroporous materials with controlled individual pore sizes and pore structures, though several methods have been reported by combining the individual technologies of mesopore and macropore synthesis, for example, by dual templating of surfactants and colloid crystals [12].

Carbon-based well organized porous materials have recently attracted intensive research due to the important application potential in gas storage and separation, fuel cell development and energy storage. This kind of materials has firstly and mainly been prepared by so-called the nanocasting

or nanoreplication method [13–17] where mesoporous silicas served as templates to create pure carbon mesoporous materials. This method consists in the impregnation of silica-based mesoporous materials with a carbon source like sucrose followed by pyrolysis and carbonisation. The silica framework is then dissolved in a solution of HF to give highly ordered pure carbon mesoporous materials which are the real replica of starting silica mesoporous templates. New methods by using a chemical vapour deposition have recently been developed. However, no hierarchically porous carbon materials containing pores of at least two different length scales have been reported.

In this paper, our first attention will be devoted to the description of different modern synthesis pathways to nanostructured mesoporous silicas, aluminosilicates, metal oxides and also pure carbon materials. Due to the important potential in catalysis applications, a special emphasis is made on the study of the thermal stability and water resistance of some of the above mentioned materials. By following closely the changes in textural, structural and morphological properties, a realistic mechanism describing the structure evolution in boiling water of mesoporous silicas and aluminosilicates will be postulated. Hierarchically meso-macroporous materials are new kinds of frameworks with important perspectives in applications. A section will describe our recently developed "template-free" self-formation strategy of porous hierarchy. An accent will be paid on our latest success about the synthesis of novel meso-macroporous carbon materials which have never been reported. In the last section, a series of new perspectives for the applications of these materials in nanotechnology, biotechnology, information technology and medical purposes will be proposed and illustrated by selected examples. We are convinced that these highly promising materials will be the new motors to induce a new wave of revolutionary discoveries in the innovation of our current industry, in the development of our modern society, in the protection of our nature and in the improvement of our human life.

2. Conception of nanostructured mesoporous materials

2.1. Development of a new low-cost and environmental-friendly synthesis pathway toward highly ordered mesoporous silicas and aluminosilicates

The development of new highly efficient, low cost and environmentally benign processes requires new materials with enhanced properties [18, 19]. As described above, zeolites [20] are very attractive because of their high capacity for ion-exchange and high internal surface and pore volume available for adsorption and catalytic reactions. However, their small openings (<1.5 nm) constitute a drawback in the treatment of heavy gasoil fractions and also in the catalytic synthesis of bulky molecules. Since the first preparation of mesoporous compounds, with openings of about 2 nm (MCM-41, 48 and 50) [4, 5], a considerable amount of work has been carried out in the field of mesoporous materials design, in particular in order to understand their synthesis mechanism, to adjust the accessible surface area and the pore sizes, to tune the atomic composition of the frameworks, to enhance their stability,… [21–28].

Most of the syntheses of mesoporous materials make use of an ionic surfactant. A new approach has been proposed on the basis of the use of non-ionic polyoxyethylene alkyl ether templating molecules [29–38] which are biodegradable and less toxic and can more easily be removed from the inorganic framework than their ionic counterparts [22–28]. The polyoxyethylene alkyl ether type surfactants have been largely used in the conception of mesoporous silicas and metal oxides [6, 7, 29–45]. In our laboratory, a large set of syntheses using $C_m(EO)_n$ (m = 6–20 and n = 8–24, in particular, $C_{13}(EO)_6$, $C_{13}(EO)_{12}$, $C_{13}(EO)_{18}$, $C_{16}(EO)_{10}$ and $C_{18}(EO)_{10}$) have been carried out [39–45]. We also tried to improve the structural order of the silica channels by adding transition metal cations to the micellar solution.

2.1.1. Pure silica mesoporous materials

On the basis of a large series of systematic studies, a relationship has been established between the initial morphology of the micelles in solution and the structure of the final materials [40–45]. High surfactant concentrations lead to the formation of a hexagonal micellar phase in solution. The final materials are however wormhole-like. Conversely, diluted micellar solutions containing only isolated spherical and cylindrical micelles in solution lead to highly ordered hexagonal stackings of channels. These

materials possess very homogeneous pore sizes centred between 4 and 5 nm and their morphology is made of uniformly sized spheres of 1–2 µm (*Fig. 1*). Due to the originality of the preparation pathway, these materials were called as CMI-1 and 3 (Chimie des Matériaux Inorganiques), depending on the non-ionic surfactant used, decaoxyethylene cetyl ether [$C_{16}(EO)_{10}$] and decaoxyethylene oleyl ether respectively [$C_{18}(EO)_{10}$] [40–45]. These observations have led us to propose two different synthesis mechanisms, depending on whether the micelles in solution have a hexagonal structure or are isolated [46–48]. In the latter case, the materials probably result from a cooperative mechanism of surfactant-silica interactions and inorganics polymerisation.

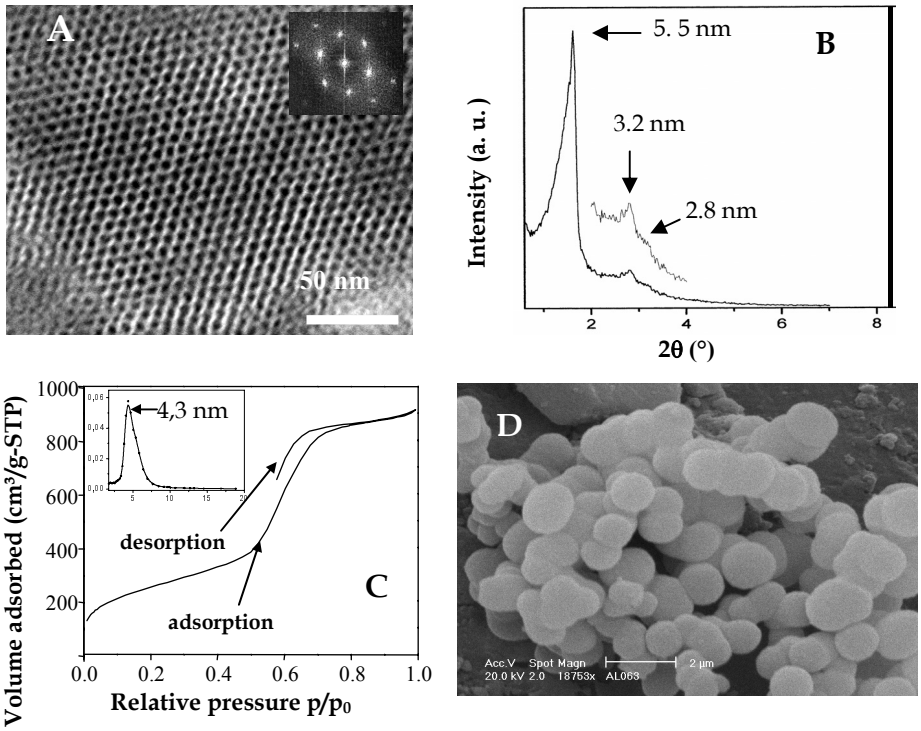

Fig. 1. Internal channel structure (A), XRD pattern (B), N_2 adsorption–desorption isotherm (C) and external morphology (D) of CMI-1 mesoporous materials

Further studies have then been carried out in order to better understand the formation of the CMI-1 materials and the influence of several preparation parameters on their final characteristics [47, 48]. We have shown that the higher the content of inorganics, the better resolved hexagonal

structure. Besides, elevated concentrations of silica precursors lead to the formation of "exotic" gyroidal, toroidal and rope-like morphologies (*Fig. 2*) [47].

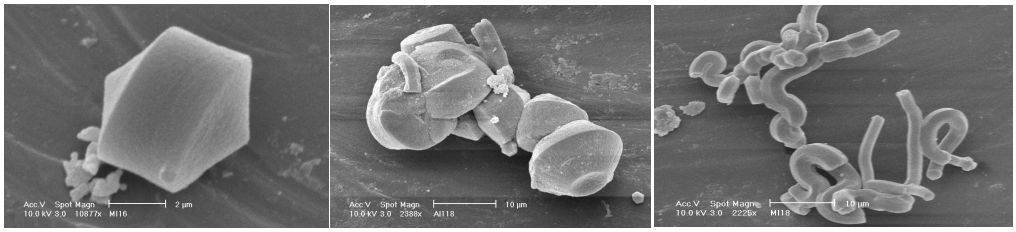

Fig. 2. Typical "exotic" morphologies of CMI-1 mesoporous materials

The pH value of the starting micellar solution was also varied [48]. The results obtained clearly prove that the hexagonal structures can be prepared in acidic as well as neutral or basic media. This shows that the proposed cooperative mechanism takes place in the whole investigated pH range and that the interactions between surfactant and inorganics are not disturbed by this parameter. Differences appear, however, from the textural and morphological point of view. As the pH value is increased, the particles become much smaller in size (submicrometric particles) and a considerable amount of secondary, interparticle porosity is observed. This is very interesting since the catalytic efficiency is enhanced by facilitated diffusion within such a framework.

The hydrothermal treatment conditions in the autoclave as well as the stirring speed of the gel were also shown to greatly influence the structure as well the texture of the materials.

This whole set of studies carried out on the preparation of silica mesoporous materials enables us to define large scale synthesis conditions depending on the desired characteristics of the final mesoporous structures. The study about the synthesis at 1 kg scale demonstrated that our synthesis protocol is well suitable for industrial production of CMI–1-type mesoporous materials.

A second preparation pathway towards highly ordered structures, but this time with concentrated surfactant solutions, was developed following the procedure described by Zhang et al. [49]. This is based on the electrostatic control of the surfactant-silica assembly by complexation of transition metal cations by the hydrophilic oxyethylene heads of the non-ionic surfactant.

Hexagonally ordered CMI-2 and CMI-4 wt.% mesoporous materials have been prepared by adding Co^{2+} cations to 50 wt.% solutions of $C_{16}(EO)_{10}$ and $C_{18}(EO)_{10}$ solutions respectively [45, 50, 51]. These materials show properties very similar to those of CMI-1 and CMI-3, except for the external morphology of the particles. The metallic cations, in addition to conferring an electrostatic character to the surfactant-inorganics assembly, probably also induce changes in the packing parameter of the surfactant molecules, which in turn is known to affect the structure of the final porous materials [7]. This study reveals very interesting in the sense that the domain of surfactant concentrations available for ordered structures synthesis is widened.

2.1.1.2. Direct synthesis of aluminosilicate Al-CMI-1 mesoporous materials

As zeolites, an aluminosilicate framework would show Brønsted acid sites due to the introduction of a trivalent aluminium atom in a tetravalent site, which creates a negative charge that can be compensated by protons. Such materials can potentially be used in catalytic cracking of gas oil and in fine chemistry syntheses [52–60].

The synthesis scheme of CMI-1 materials has been used with supplementary addition of an aluminium source. The results show that the presence of this additional species needs reoptimisation of preparation conditions. In particular, the hydrothermal treatment conditions had to be re-evaluated for obtaining ordered mesoporous structures. The preparation pH as well as the silica/alumina molar ratio have also been varied. High quality materials can be prepared with elevated initial aluminium contents and with all the atoms incorporated within the walls of the porous frameworks (*Fig. 3*). The channels are stacked hexagonally and the pore sizes are very homogeneous and similar to the pure silica counterparts. In some cases, hollow spheres as well as macropores have been observed, but no definite explanation has been found to describe their formation. The adsorption of basic molecules (ammonia, methylamine,…) revealed quite a weak interaction with the framework, suggesting that the Al atoms are not present on the internal surface of the pores, but probably buried inside the thick walls separating adjacent mesopores [61].

As for the pure silica CMI-1-type materials, the protocol has been extended to the preparation of 1 kg of final material at once. It appears to be very suitable for the industrial preparation of mesoporous materials with the desired final characteristics.

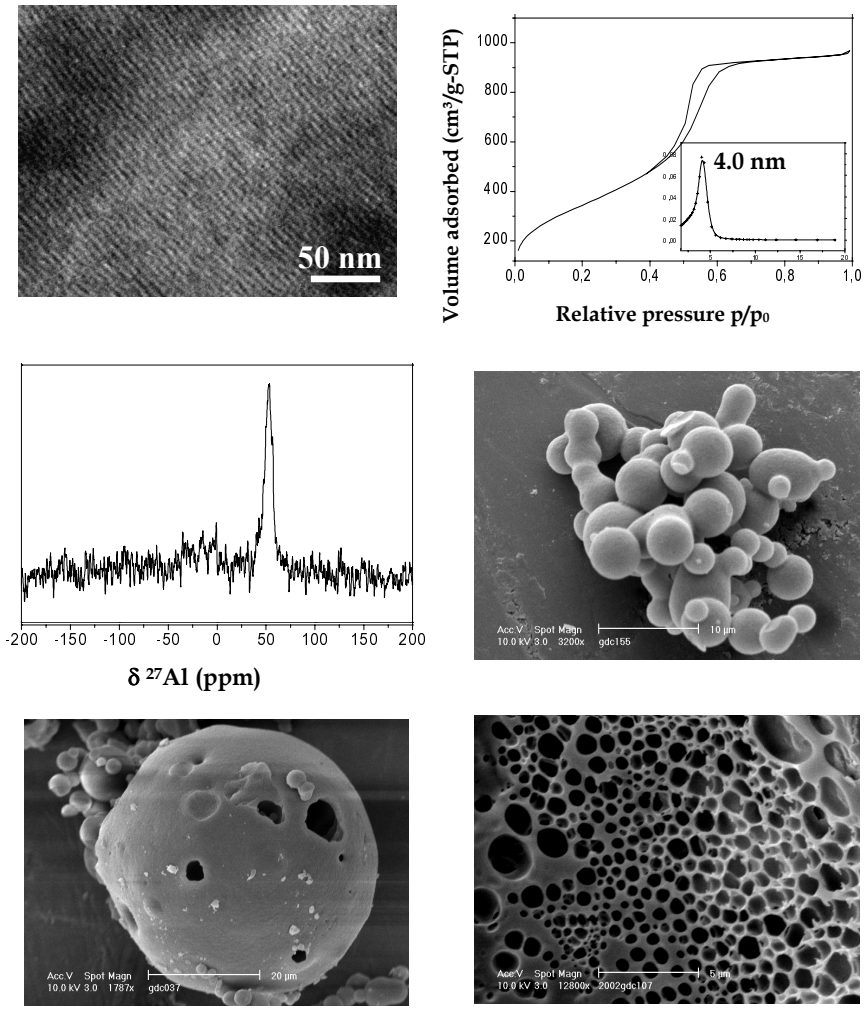

Fig. 3. Structural, textural and morphological features of aluminosilicate Al-CMI-1 mesoporous materials

2.1.3. Thermal stability and boiling water resistance of pure silica and aluminosilicate CMI-1 mesoporous materials

Other than porosity, the thermal and boiling water resistance of materials are crucial for industrial applications. The behaviour of CMI-1 materials was thus firstly investigated upon calcinations under oxygen. The results clearly show that the mesostructure as well as the textural characteristics are maintained until 1000 °C for the pure silica and 950 °C for the

aluminosilicate materials. This is different from analogues prepared via ionic templating, which collapse at temperatures higher than 650 °C, and the higher thermal stability of CMI-1 can be attributed to the thicker pore walls separating adjacent mesopores. In the case of our aluminosilicate structures, no dealumination upon calcination is observed in contrary to the Al-MCM-41 analogues, this behaviour can be attributed to the fact that the Al atoms are buried inside the silica walls.

The boiling water resistance has been evaluated by immersing materials in boiling water [62]. Samples were then withdrawn after defined durations ranging from 5 minutes to 90 hours. In this case, we observed a different behaviour for silica and aluminosilicate CMI-1 materials.

For the pure silica, the structure is immediately affected in contact with the hot water. Nevertheless, hexagonal ordered zones can still locally be distinguished by microscopy, indicating that there is some maintain of the main framework. Severe changes appear from the textural point of view. The specific surface area as well as the pore sizes immediately decrease after immersion while nearly the same textural characteristics as the starting materials are recovered after longer durations in boiling water. This evolution has been described for the first time. We postulated a mechanism based on the rapid hydrolysis of internal surface species, partially blocking the openings (*Fig. 4*). Then, these species dissolve into solution, leaving again a porous structure with high specific surface areas and pore sizes. For very long immersions, the surfaces continue to be eroded, leading to the ultimate destruction and collapse of the structure.

The aluminosilicate materials show the same initial evolution as their pure silica counterparts immediately after immersion in boiling water (*Fig. 5*). However, for the longer durations, the frameworks do not undergo further alteration, leaving an intact framework even for the very long immersions [63]. It is possible that the inner surface of the pores is pure silica and that Al atoms are buried within the thick walls. This silica inner surface is hydrolyzed as for pure silica structures immediately after immersion. However, when these species dissolve into solution, Al atoms become exposed on the inner surface of the channels. These then play a protecting role by repelling the attack of water molecules, as already described in literature, which thus leaves a more or less intact structure after further immersion, even for very long times up to 90 hours.

These results supply important information concerning the possible use of mesoporous materials in aqueous media and can guide us to use them under best realistic conditions.

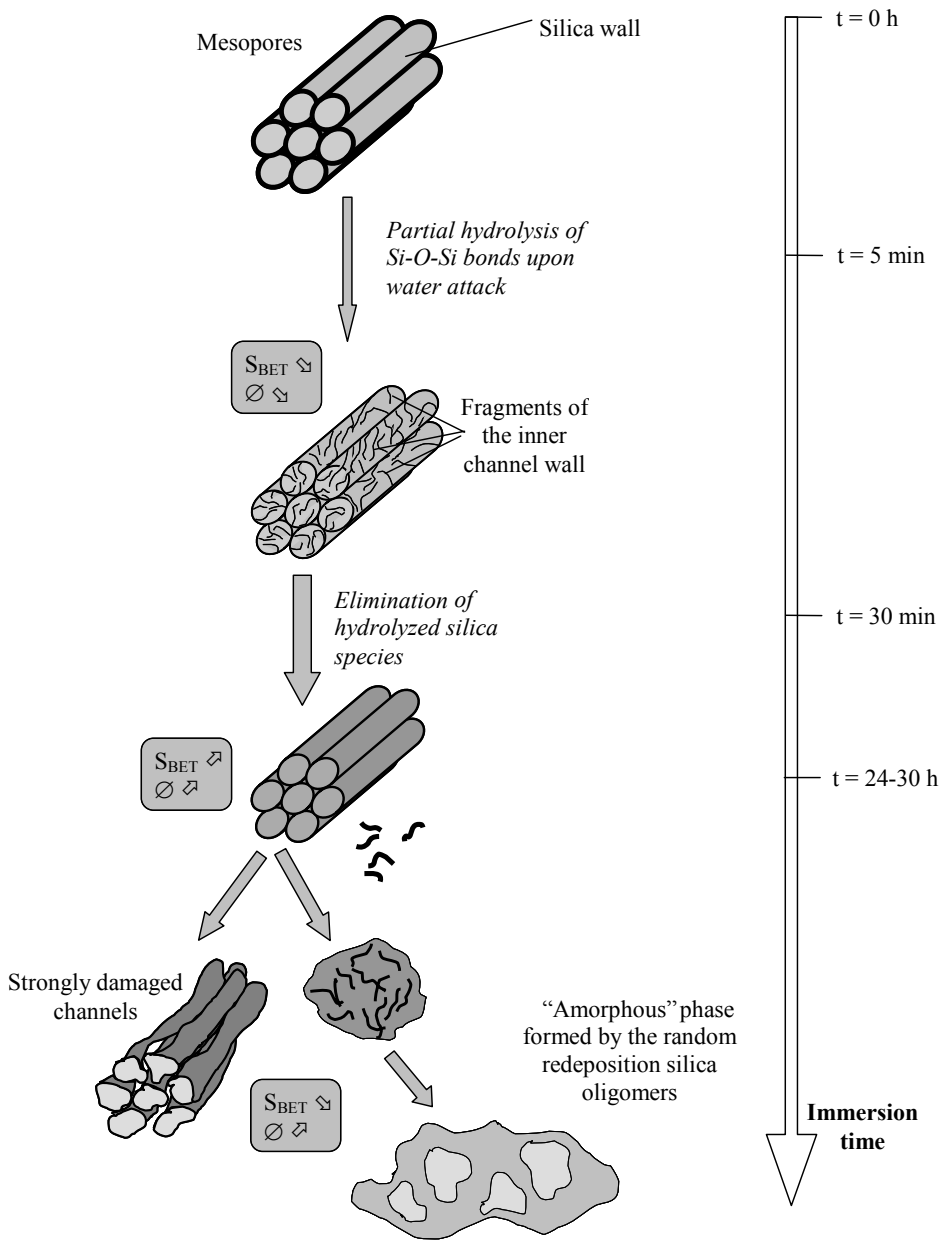

Fig. 4. Evolution of pure silica CMI-1 mesoporous materials as a function of time in boiling water

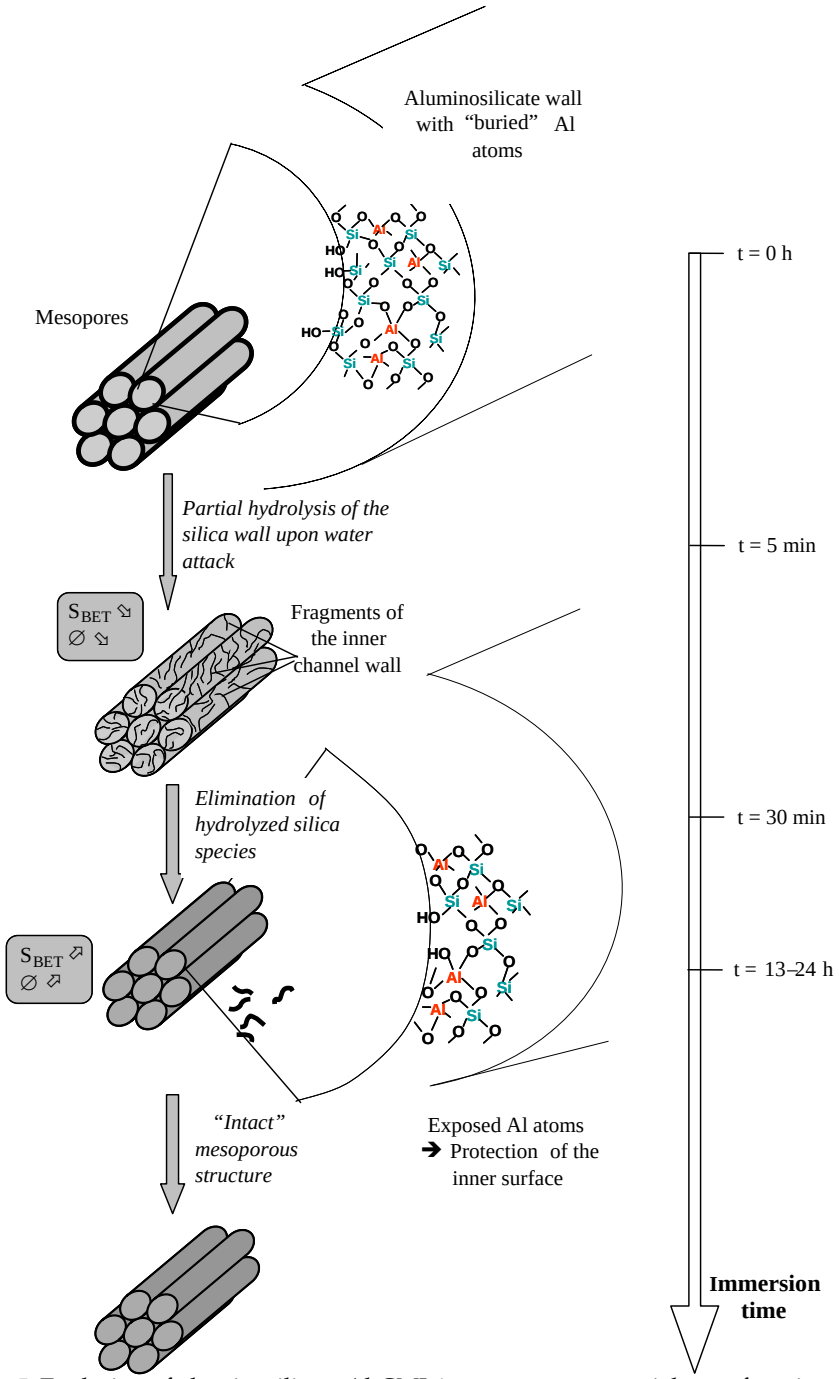

Fig. 5. Evolution of aluminosilicate Al-CMI-1 mesoporous materials as a function of time in boiling water

2.2. Highly ordered single and bi-transition metallic ions incorporated silica mesoporous materials

The increasing needs of efficient and selective catalysts as well as the fundamental investigations are continuously driving the forces for the synthesis of new performant catalytic materials. Hexagonal mesoporous materials offer new opportunities for transition-metal incorporation into silica framework. It is possible to obtain highly dispersed and isolated

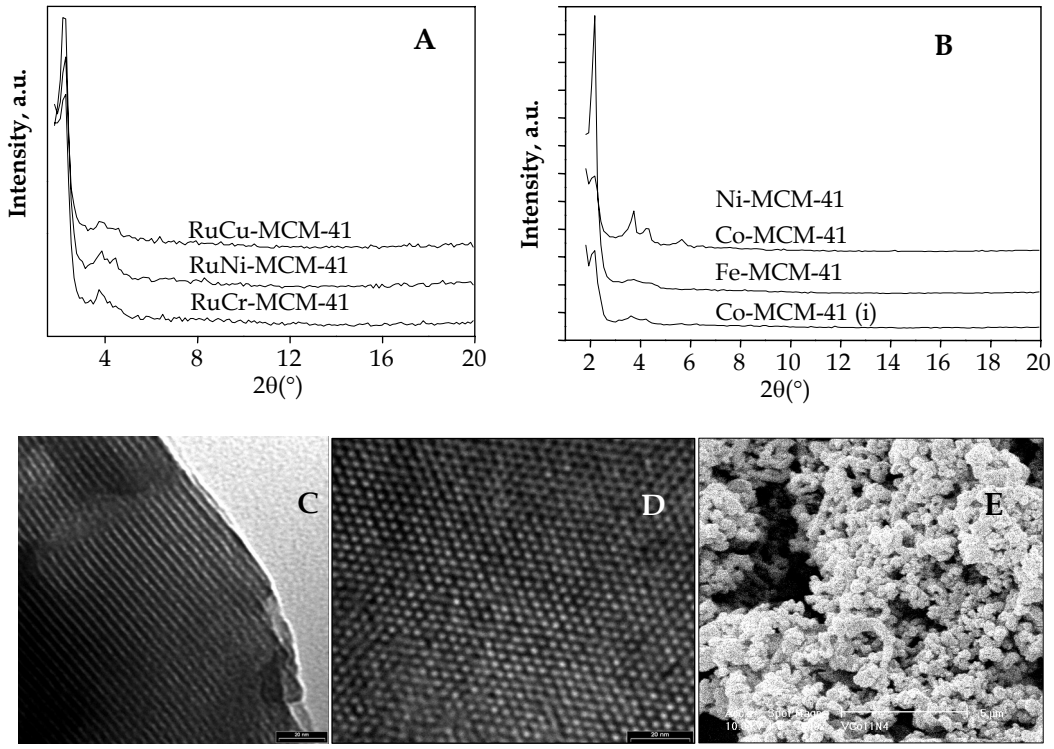

Fig. 6. XRD patterns (A and B), TEM (C and D) and SEM (E) images of mono- (B, C, D and E) or bi- (A, C, D and E) transition metallic ions modified mesoporous silicas

active sites in a silica framework. In addition, silica mesoporous molecular sieves contain a large number of silanol groups at the surface of their channels, a wide variety of reactive metal species can therefore be anchored on the surface by reaction with the silanol groups. In our laboratory, by direct synthesis with two different silica sources (sodium silicate and TEOS), a large series of transition metal ions such as Ti, V, Cr, Fe, Co, Ni,

Mn, Cu, La, Ru were incorporated into the mesoporous silica frameworks [64–70]. The obtained materials have been used as catalysts in the liquid phase selective oxidation reaction of styrene, benzene and alcohols and shown the remarkable catalytic activity under mild conditions. Some of these metal ions gave a high catalytic conversion but low selectivity; others led to the inverse results. The incorporation of two different metals might therefore create new materials with different or new redox and acid properties. Some combinations of two metals [71–79] such as Co–V, Co–Nb, Co–La, Mn–La, Ni–Ru, Ni–Cr, Ni–Ti, V–Ti, V–Cu, V–Co, V–Ti, Nb–Ti, Ru–Cr and Ru–Cu have been explored.

The highly ordered mesoporous silicas can be obtained whatever mono or bimetallic ions with hexagonal arrangement of their cylindrical channels and very narrow pore size distributions as confirmed by XRD (*Fig. 6A* and *B*) and TEM techniques (*Fig. 6C* and *D*). The morphology of single or bimetallic ions containing structures (*Fig. 6E*) is quite similar with globular spheres of 100–300 nm in size.

2.3. Nanostructured mesoporous metal oxides

Due to the large field of applications ranging from catalysis to ceramics, among the non-silica mesoporous oxides, zirconia is of particular interest. ZrO_2 can catalyze or is a catalyst support for various reactions such as the catalytic reduction of aldehydes and ketones with 2-propanol [80] or the hydrogenation of aromatic carboxylic acids [81]. Using cationic [82], amphoteric [83], anionic [84], or neutral [85–89] templates and, depending on the synthesis pathway, zirconyl chloride or zirconium propoxide as zirconium precursors, hexagonal, cubic or disordered mesoporous zirconia were successfully obtained. A systematic kinetic study of mesoporous zirconia formation has been performed in our laboratory [86–89] in order to optimize the synthesis conditions by using cetyltrimethylammonium bromide as surfactant and zirconyl chloride as inorganic source. The broad reflection line in the range of $25° < 2\theta < 40°$ observed in XRD patterns indicates the amorphous nature of our ZrO_2 materials. The TEM picture of a typical sample shows a quite porous system (*Fig. 7*). The present study reveals that zirconia molecular sieves can be obtained via an electrostatic assembly. The recovered molecular sieves exhibit specific surface areas up to 300 m^2/g and uniform pore diameters.

Titanium dioxide and iron oxides and oxyhydroxides are of technological importance as (photo)catalytic materials, sorbents, pigments, flocculents, coating, gas sensors and ion exchangers. In our laboratory, hollow

microspheres of mesoporous titania with a thin shell of anatase structure have been prepared by using poly(ethylene oxide) assisted nanoparticle assembly in a non-aqueous system. A high surface area of 378 m^2/g and pore volume of 0.34 cm^3/g was obtained in the as-prepared sample with a pore size of 2.6 nm [90]. A new mesoporous form of crystalline β-FeOOH (akaganeite) was also successfully prepared. The synthesized mesoporous

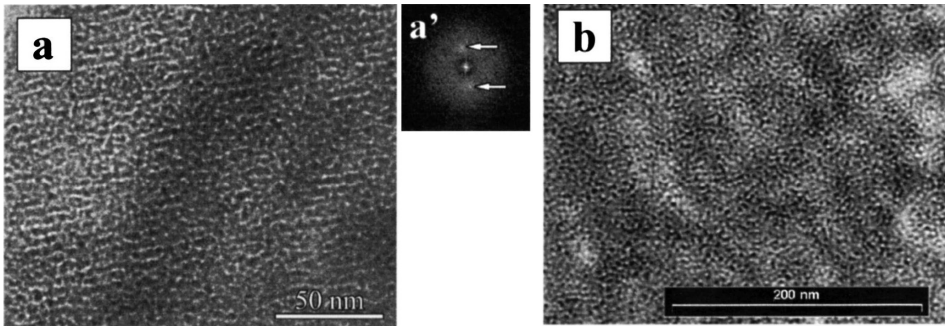

Fig. 7. TEM micrographs (a and b) and their Fourier transform (a′) of mesoporous ZrO_2 materials

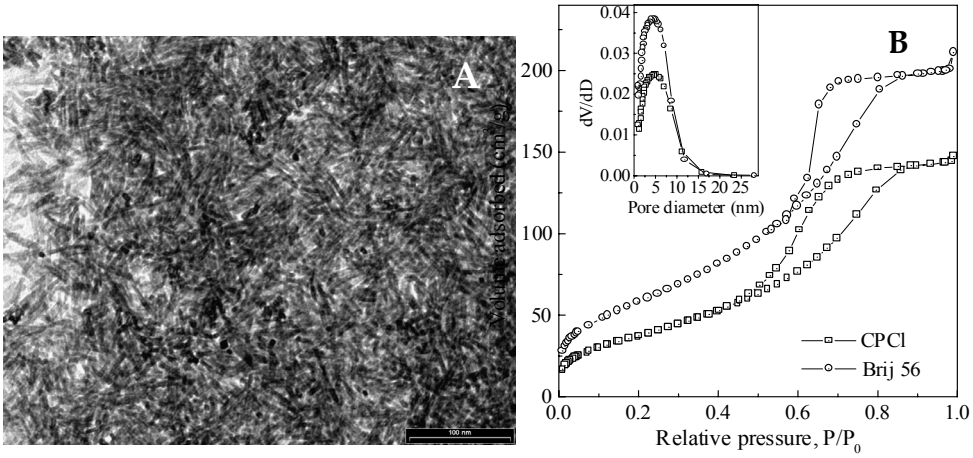

Fig. 8. TEM image (A) and N_2 adsorption–desorption isotherms (B) of mesoporous crystalline iron oxide materials synthesized with CPCl and Brij 56, and the corresponding pore size distribution curves (*inset of B*)

β-FeOOH has a high surface area of 228 m^2/g and a pore size of 4.3 nm with a hierarchical scaffold-like structure formed through the aggregation and intergrowth of akaganeite nanorods (*Fig. 8*) [91].

2.4. Highly ordered mesoporous carbon CMI-8: nanocasting of silica CMI-1 materials

A few years ago, Ryoo et al. reported the first synthesis of new type of mesoscopally ordered mesoporous carbon molecular sieves designated as CMK-1 by polymerizing a carbon source inside the pores of a cubic silica MCM-48 material [4, 13–17, 92, 93]. Later, other mesoporous carbons were prepared by using various kinds of templates such as SBA-15 [15], MSU-H [94], HMS [95] and MSU-1 [96].

The synthesis of ordered mesoporous carbon materials designated as CMI-8 was also made by impregnation of an aqueous acidic sucrose solution into the hexagonally stacked mesopores of a CMI-1 silica material. The impregnated sucrose was then converted to carbon inside the mesochannels by a heat treatment, followed by a pyrolysis step under nitrogen. The carbon replica was finally obtained after dissolution of the inorganic network.

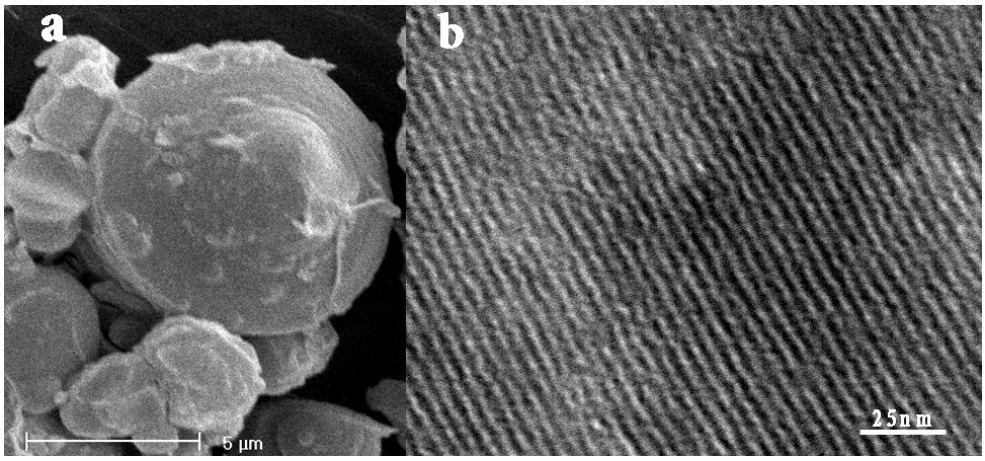

Fig. 9. SEM (a) and TEM (b) images of the mesoporous carbon CMI-8

The SEM characterisation of the CMI-8 shows that the morphology of this new carbon structure is exactly the replica of the CMI-1 used as template (*Fig. 9a*). The structural replication is confirmed by the regular array of channels observed by TEM (*Fig. 9b*). XRD measurements evidence the hexagonal stacking of the channels as three diffraction peaks could be assigned to (100), (110) and (200) reflections of the 2-d hexagonal space

group (p6mm). From the textural point of view, the carbon replica shows a type IV isotherm, characteristic of mesoporous structures and the narrow pore size distribution is centred at 2.2 nm. A high surface area and total pore volume of respectively 1653 m^2/g and 0.86 cm^3/g were obtained.

These results show that new ordered mesoporous carbon materials with particular CMI-1 morphologies can successfully be synthesised by using a modified nanocasting pathway.

2.5. Conclusions

Low-cost and biodegradable non-ionic surfactants turn out to be very suitable for the conception of highly ordered homogeneous mesoporous materials. This synthesis pathway is also very versatile as it can easily be tuned depending on the desired final structures, textures and morphologies. These developed materials are currently studied for numerous applications in nanotechnology and biotechnology as will be described in more detail further in this review. The non-ionic synthesis route is also suitable for the preparation of aluminosilicate frameworks, which, as their silica analogues, show remarkable thermal and boiling water stabilities. Finally, all-silica CMI-1 materials have successfully been employed as templates for the conception of highly structured mesoporous carbons, which also show a great potential in new technological developments.

3. From mesoporous materials to hierarchical multiporous structures

In order to improve and develop new catalytic processes, unprecedented materials, which integrate several functionalities or hierarchical pore systems into one single body, have to be conceived [97–105]. Nature tells us that hierarchy is essential to life. Trees have a hierarchical structure from the stem to the leaves, the respiratory system and blood circulation in human bodies range from large vessels to very small capillaries. For catalysis, the combination of different pore systems thus allows efficient transport of guest molecules and could also account for the realisation of distinct (and eventually successive) reaction steps within one single catalyst.

Macro-mesoporous catalysts or catalyst supports with different atomic compositions of their frameworks have already been reported [99–117]. The most employed preparation route is a rather tedious dual-templating scheme. For example, it makes use of latex spheres as templates for the macropores whereas the mesopores are created by micelle-directed assem-

blies [8, 9, 110]. This pathway requires a calcination to remove the templates from the openings, but many oxide compositions suffer from sintering and collapse upon such a treatment. Other reported original preparations make use of bacteria-filaments, phase separation, vesicle formation or multi-surfactant templating for porosity creation [111–118]. All of these methods however suffer from a difficult control in the homogeneity of the openings within the final structures. That is why we developed new and simple preparation routes, based on the rapid polycondensation of inorganic precursors, i.e. a self-generation of porous hierarchy. Like the mesoporous materials, several hierarchical metal oxides have been used as templates for exploring the possibility to create multi-scaled porous carbons. Such structures which we labelled as CMI-7 would be of considerable interest due to their unique controlled bimodal pore-system and offer very interesting perspectives in nanocasting processes leading to unprecedented hierarchical metal oxides [99–105, 119, 120].

3.1. Meso-macroporous aluminosilicates CMI-7-SiAl

Porous aluminosilicate compositions can find many applications in catalytic processes. Catalytic cracking of heavy petroleum feedstocks and fine chemistry acid-syntheses are only the main examples for this. The existing processes could significantly be improved if the low-surface area "amorphous" aluminosilicates, which are actually employed, could be replaced by homogeneous hierarchical macro-mesoporous structures.

Our first meso-macroporous aluminosilicate materials were prepared via a single surfactant-assisted pathway. Materials made of macrochannels separated by disordered mesoporous aluminosilicate walls were obtained [119]. The same macro-mesoporous structures can even spontaneously be formed without any templating molecule. This suggests that the dual pore system may result from the polymerisation chemistry of the inorganic sources in solution [120]. The materials are made of tubular macrochannels with openings ranging from 0.5 to 2 μm, separated by wormhole-like disordered mesopores of about 4 nm in diameter (*Fig. 10*). The regularity in size of the macrochannels is demonstrated by the cross-section observed by TEM. The walls separating the tubes are amorphous and a large deal of Al atoms are incorporated in tetrahedral framework positions as evidenced from ^{27}Al NMR measurements. We proposed a synthesis scheme implying the rapid mineralisation of the inorganics around water–alcohol channels that form due to the hydrodynamic flow of the solvent [119–121]. The mesopores result from the spaces left between the rapidly formed

aluminosilicate nanoparticles. Whatever pH of the starting aqueous solution is, macropores always form but mesopores are much more homogeneous in acidic conditions. When comparing with the materials prepared in the presence of a surfactant, it appears that the latter facilitates the incorporation of Al atoms in tetrahedral positions and also induces more regularity within the mesoporous part of the compound, but its exact role still remains to be clarified.

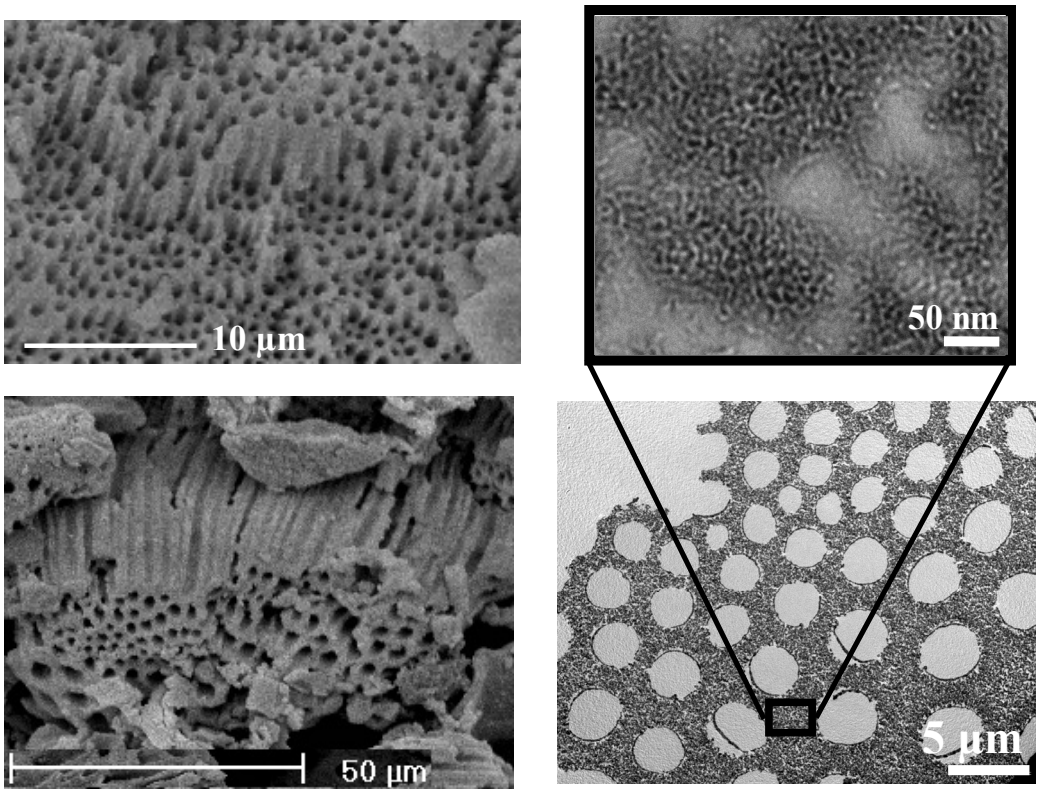

Fig. 10. SEM and TEM images of meso-macroporous aluminosilicates illustrating the macrochannels, their cross-section and their mesoporous walls

The results clearly show that the control of the hydrolysis and polymerisation kinetics of the inorganic sources in solution is a powerful tool to fabricate hierarchical macro-mesoporous materials without needing complex templating procedures.

3.2. Meso-macroporous and micro-macroporous Zirconium oxides CMI-7-Zr

Zirconium oxide porous structures are particularly interesting because of their high thermal stability, being potentially applicable as catalyst supports [122], adsorbents [123], heavy duty membranes [124] and chemical sensors [125]. We demonstrate here a simple procedure for the synthesis of uniform meso-macroporous and micro-macroporous zirconium oxides either in the presence of surfactant (Brij 56 [126] or CTMABr [127]) or without any templating agent. Two types of zirconium alkoxides ($Zr(OC_3H_7)_4$ or $Zr(OC_4H_9)_4$) were used as inorganic precursors. The particles synthesised by polymerisation of zirconium propoxide with or without surfactant are mainly tens of micrometers in size with a regular array of macropores of 300–500 nm in diameter. The walls separating the macropores additionally exhibit accessible mesochannels (around 2.0 nm) with a wormhole-like array. This is in accordance with the observations made for aluminosilicate materials as described above. The main difference relies in the shape of the macropores as well as in the sizes of the mesopores, which are quite smaller in the present case. Nevertheless, the N_2 adsorption–desorption isotherms are of type IV, characteristic of mesoporous structures, with a high specific surface area of about 700 m^2/g. The wide-angle XRD patterns of the a-synthesized zirconia reveal an amorphous zirconia framework, which is again in accordance with the observations made for aluminosilicate meso-macroporous structures.

The use of zirconium butoxide leads to macrochannels with slight sinusoidal shapes and diameters ranging from 300 to 800 nm. Again, the amorphous walls separating adjacent macropores exhibit disordered mesochannels (~2.0 nm). The textural characteristics are not affected by the change in the inorganic alkoxide precursor.

As for the aluminosilicates, these syntheses depend obviously upon the hydrolysis and the condensation of the zirconia precursors. In this way, a controlled synthesis of hierarchical porous zirconium was carried out by a careful control of the polymerisation of zirconia propoxide precursor drops. The SEM pictures reveal 2 mm-sized zirconia particles with a unique "mexican-hood"-like morphology (*Fig. 11a*). The particles are characterized by a dense smooth surface, below which an extremely interesting and regular array of macropores is observed (*Fig. 11b*). The macrochannels are parallel to each other, funnel-like shaped and perpendicular to the tangent of the smooth surface. The TEM observations confirm the presence of macropores (*Fig. 11c*), with disordered meso- and microporous walls (*Fig. 11d*). The yield of the reaction is nearly 100%.

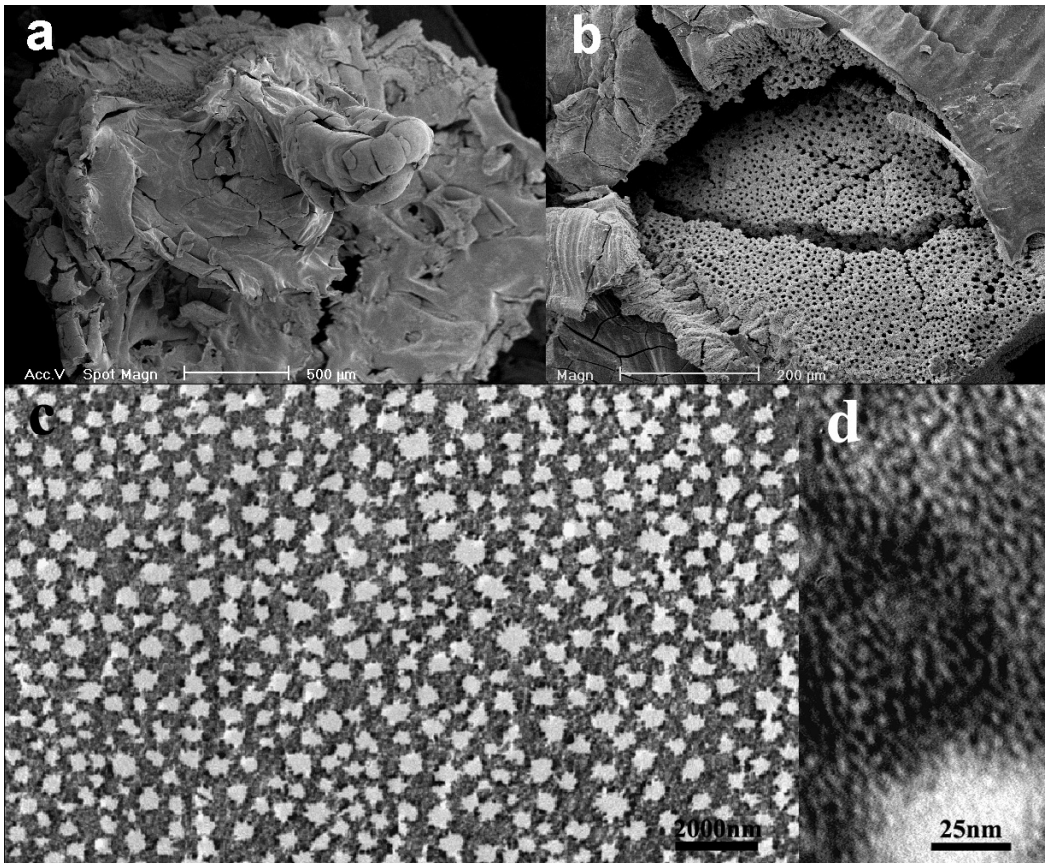

Fig. 11. Representative SEM images (a) of the mexican-hood-like morphology and the regular macrochannels (b) of the meso-macroporous zirconia; (c) is the cross-sectional TEM image of the macropores viewed perpendicular to the pores; (d) is the high magnification TEM image of the macropore walls showing the wormhole-like mesostructure

A new type of hierarchically three-length-scaled porous zirconium oxide was also synthesised by a simple one-pot method with single alkyltrimethylammonium surfactant templating [128]. The structures exhibit a uniform array of macrochannels (300–500 nm) with walls formed by an assembly of supermicroporous nanoparticles (25 nm sized) with irregular mesovoids. A very high surface area of 903 m^2/g is obtained with a total pore volume of 1.0 cm^3/g.

3.3. Micro-macroporous Titanium oxides CMI-7-Ti

Titanium oxides are interesting compositions because of their applications in photocatalysis and as catalyst supports. Mesoporous Ti oxides have been prepared by several surfactant-assisted pathways, with control of channel structure, texture and morphology [99, 105, 118, 129–134]. The synthesis

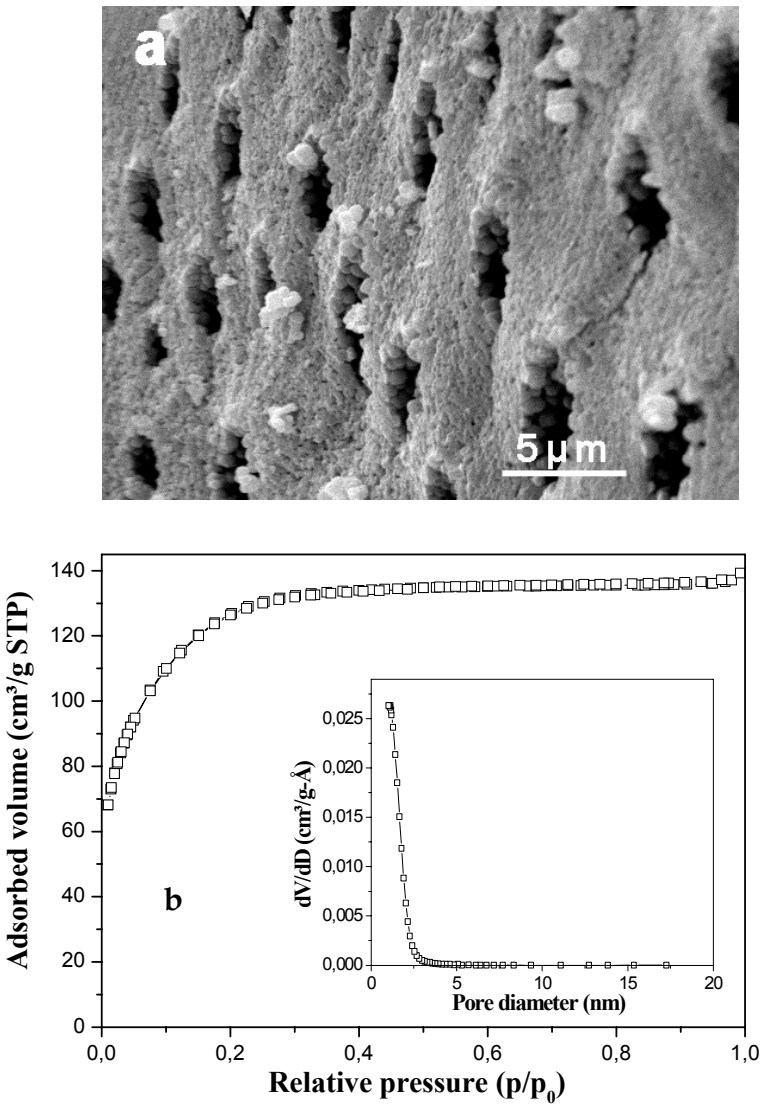

Fig. 12. SEM micrography (a), adsorption–desorption isotherm and pore size distribution (b) of a micro-macroporous titanium oxide synthesised via $Ti(OEt)_4$

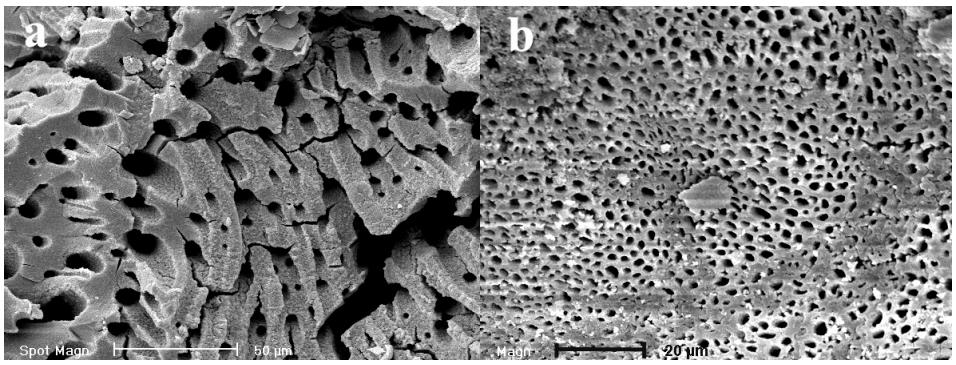

Fig. 13. SEM pictures of the micro-macroporous niobia (a) and meso-macroporous yttria (b)

of high surface area hierarchical micro-macroporous titanium oxide materials was carried out by a controlled polymerisation of titanium alkoxide inorganic sources [$Ti(OC_2H_5)_4$, $Ti(OC_3H_7)_4$, $Ti(OC_4H_9)_4$]. The synthesized particles are around 1 mm in size and exhibit a regular array of funnel-like sinusoidal macrochannels (*Fig. 12a*). The macropores sizes range from 0.3 to 1.5 µm and their walls are formed by an agglomeration of microporous TiO_2 nanoparticles. This microporosity is confirmed by type I N_2 adsorption–desorption isotherms (*Fig. 12b*). Very high surface areas (400–470 m^2/g) are obtained for each titanium alkoxide precursor and the pore size distribution is always centred in the microporous range.

Ethylene photodegradation was employed as a probe reaction to evaluate the photocatalytic activity of these new meso-macroporous titanium oxide structures. The results reveal a photocatalytic activity of 60% much higher than that of commercial P25 Titania powders [135]. It is evident that these new TiO_2 bimodal meso-macroporous structures are of promising catalysts and catalyst supports.

3.4. Micro-macroporous Niobium oxides CMI-7-Nb

Few years ago, Antonelli reported the synthesis of meso-macroporous niobium oxides by a NaCl-promoted vesicle templating method using a niobium ethoxide/amine gel [111]. These materials have macropore sizes in the 200–300 nm range and mesopores around 2 nm. Despite their interesting structural and textural properties, these structures can only be prepared by quite a complex synthesis route. In our laboratory the self-formation pathway used for the zirconia and titania was applied to the conception of

hierarchical micro-macroporous niobium oxides. The preparations were carried out at different starting pH values (2, 7 and 12). In each case, the synthesised Nb_2O_5 particles are mainly 100 μm in size with a regular array of parallel macropores (*Fig. 13a*). They extend through almost the whole particle and their diameter ranges from 0.3 to 10 μm. Moreover, high magnification TEM images reveal accessible micropores in the macropore walls. XRD patterns show broad features in the 2θ range of 20–40° and 40–60°, indicating the global amorphous nature of the niobium oxide frameworks. Type II isotherms, typical of macroporous structures, are observed and the BET surface areas are 144, 127 and 73 m^2/g for the syntheses carried out in acidic, neutral and basic media respectively. Finally, a TG/DTA analysis demonstrates the strong acidic properties of the hydrated hierarchical micro-macroporous niobium oxide. In the future these new solid catalysts will be tested in low temperature catalytic reactions [136].

3.5. Meso-macroporous Yttrium oxides CMI-7-Y

Yttrium oxides possess unique properties, the main ones being its higher melting temperature than many other well-known oxides, a wide energy bandgap, high values of electrical resistivity and electric strength [137]. The self-formation strategy was also applied to the preparation of hierarchically porous Y_2O_3 by a controlled polymerisation of yttrium butoxide in aqueous media. For each tested preparation pH value, the synthesised Y_2O_3 particles are 0.5 to 2 μm in size and are covered by a smooth surface, cracked at some places. Higher resolution SEM observations of the fissured particles reveal a macrostructure below the smooth surface (*Fig. 13B*). It is worth to mention that the yield of the syntheses as well as the amount of macropores per particle continuously decrease with increasing initial synthesis pH values. The macropores are funnel-like shaped and parallel to each other, as observed for the previous zirconia and their diameters range from 1–5, 2–8 and 5–10 μm respectively for syntheses carried out in acidic, neutral and basic media, respectively. In each case, the macropore walls are formed by aggregation of mesotructured nanoparticles giving a supplementary inter-particular porosity centred at 30 nm. As for all the previously described compositeons, the meso-macroporous yttria structures are amorphous at the atomic scale. BET surface areas of 85, 74 and 94 m^2/g are obtained for samples prepared in acidic, neutral and basic media respectively, and the BJH pore size distributions are quite broad and centred in the mesopore range, 3–7 nm for syntheses carried out in acidic and neutral media and

5–15 nm in an alkaline medium. These new macro-mesoporous yttrium oxide structures will be tested as catalysts or supports in a wide range of chemical reactions [138, 139].

3. 6. Binary metal oxide composites CMI-7-M_1M_2

By using the mixed alkoxide solutions, a series of binary oxide composite materials, including titania–zirconia, titania–alumina, alumina–zirconia, zirconia–silica and alumina–silica, with a hierarchically bimodal meso–macroporous structure similar to those of single metal oxides (*Fig. 14* and *Table 1*) can be prepared [140]. In comparison with the meso–macros-

Table 1. Structural properties of some synthesized meso-macroporous binary oxide materials

Samples	Composition (mol%)				S_{BET} (m^2/g)	V_{pore} (cm^3/g)	D_{meso} (nm)	Crystal phase[a]
	Ti	Zr	Al	Si				
CMI-7-Zr	–	100	–	–	593	0.50	1.8	(amorph)
CMI-7-TiZr-1	50	50	–	–	720	0.92	2.2	(amorph)
CMI-7-Ti-Zr-2	70	30	–	–	632	0.85	2.0	An
CMI-7-Ti-Zr-3	80	20	–	–	595	1.01	3.4	An, trace of Br
CMI-7-Ti-Zr-4	90	10	–	–	213	0.60	5.6	An, trace of Br
CMI-7-Ti-Zr-5	50	50	–	–	704	0.90	2.5	trace of An
CMI-7-Ti-Al-1	70	–	30	–	571	0.89	3.5	trace of An
CMI-7-Ti-Al-2	50	–	50	–	893	1.57	2.8	(amorph)
CMI-7-Ti-Al-3	30	–	70	–	557	0.97	2.6	trace of Bo
CMI-7-Al	–	–	100	–	381	0.68	3.0	Bo
CMI-7-ZrAl-1	–	70	30	–	593	0.73	1.7	Ba
CMI-7-ZrAl-2	–	50	50	–	502	0.99	1.8	Ba
CMI-7-ZrAl-3	–	30	70	–	534	1.37	2.1	Ba, trace of Bo
CMI-7-AlSi-1	–	–	70	30	574	1.45	7.1	trace of Bo
CMI-7-AlSi-2	–	–	50	50	630	1.94	5.1	(amorph)
CMI-7-AlSi-3	–	–	30	70	518	1.12	5.2	(amorph)
CMI-7-ZrSi-1	–	70	–	30	794	0.75	1.4	(amorph)
CMI-7-ZrSi-2	–	50	–	50	597	1.38	1.1	(amorph)
CMI-7-ZrSi-3	–	30	–	70	965	2.97	n. a.	(amorph)

[a] Abbreviations: An, anatase; Br, brookite; Bo, Boehmite AlO(OH); Ba, Bayerite $Al(OH)_3$; amorph, no peaks obtained in wide-angle XRD, indicating amorphous material.

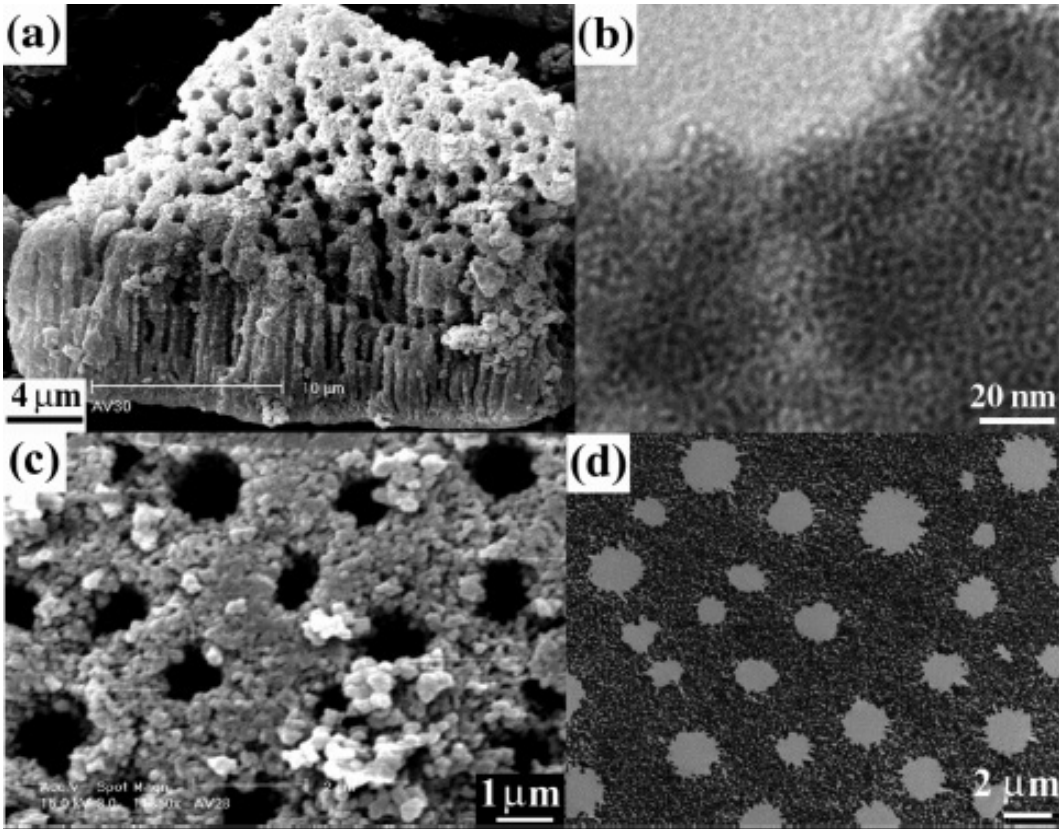

Fig. 14. SEM (a and c) and TEM (b and d) micrographs of a representative meso-macroporous binary mixed metal oxides (TiO_2–ZrO_2)

tructured macrostructured single metal oxides, the introduction of a secondary oxide leads to a significant improvement of the structural and textural properties of the resultant materials. The synthesized binary mixed oxides have a homogeneous distribution of the components and have higher surface areas than the single metal oxides. Moreover, not only the mesopore sizes, but also the macropore sizes of binary metal oxides could be tailored and controlled by the variation of the molar ratios of the metal precursors. The thermal stability of the binary oxide compositions could also be enhanced significantly. These meso-macrostructured binary oxide compositions should be significant for the use as advanced functional materials, especially in the catalysis applications.

3.7. Meso-macroporous hierarchical carbons CMI–9

Mesoporous carbons offer some interesting perspectives in applications such as hydrogen storage, adsorption, catalysis and electrodes. We expect a multi-scaled pore system to significantly broaden the application spectrum of open carbon structures. That is why we explored the possibility to apply the replication concept, successfully used for mesoporous structures, to hierarchical metal oxides [13, 92–96].

A meso-macroporous zirconia material was used as hierarchical template. In order to obtain a carbon with multi-scale porosity, it is obvious that not the whole porosity had to be filled by a carbon precursor, as after dissolution of the inorganics, only meso-openings would be left. In fact, the amount of added carbon was chosen as to fill only the mesoporous walls separating the macrochannels, which remain empty. The purity of the carbon material was studied by thermogravimetric and FTIR measurements. The characterisation results evidence that the obtained meso-macroporous carbons contain less than 1% residues, indicating an almost pure carbon framework. These two techniques also confirm the expected interesting hydrophobic properties of the prepared carbon structures.

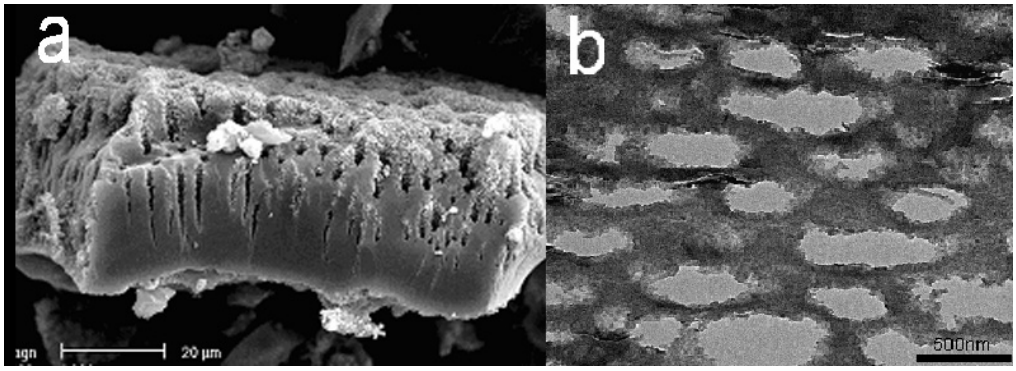

Fig. 15. SEM (a) and TEM (b) images of the hierarchical meso-macroporous carbon

The SEM image (*Fig. 15a*) clearly shows 200–600 nm sized macrochannels within the carbon particles. This macrostructure is further confirmed by the TEM observations as shown in the cross-sectional view in *Fig. 15b*. Moreover higher resolution TEM observations reveal the presence of disordered mesopores within the macropore walls. The textural characterization reveals a very high specific surface area of 860 m^2/g and homogeneous mesopores with a distribution centred at 1.8 nm. All of the

obtained results clearly show the correspondence between the morphology and structure of these carbon materials and their zirconia templates.

It is evident that the carbon replication is also suitable for being used with multi-porous structures as starting templates. Nevertheless, precise information about mesopore volume has to be taken into account for the calculation of the proper amount of carbon source to be added to the template. These new meso-macroporous carbons are expected to widen the application field of nanotubes and mesoporous analogues.

3.8. Conclusions

Hierarchical meso- (or micro-) macroporous metal oxide and aluminosilicate CMI–7 materials have been prepared by a simple, reproducible and low-cost synthesis route. The use of a surfactant helps in structuring the mesopores present within the materials. The spontaneous pathway is based on the synergy between the polymerisation kinetics of the inorganic precursors and the hydrodynamic flow of the solvent. Our route seems to be very suitable for preparing a rich variety of oxide compositions. These materials have also been used as starting templates in nanocasting processes. In particular, it has been shown that meso-macroporous carbon replica CMI–9 could be achieved by partially infiltrating the openings of the starting template. The self-formation strategy and these new hierarchically multiporous structures can open exciting avenues for the conception of new classes of nanostructured porous materials. It is expected that hierarchically micro-macroporous and meso-macroporous structures with any chemical compositions can be prepared by application of the synthesis strategy presented in this paper.

Nature is an unlimited specimen with numerous examples of exceptionally strong building materials. Despite their diversity, one nearly constant feature is that almost all biomineralized structures are highly hierarchical. These materials often show complex hierarchical organisation from the nanometer to macroscopic scale, teaching us how structural materials can assemble themselves. Nature, supplying multiple lessons of self-formation of hierarchy, is therefore the source of new strategy inspiration [141, 142]. Our laboratory continuously works in this direction to supply more synthesis strategies for the conception of more sophisticated materials and more understanding and more knowledge to shed light in the synthesis mechanisms. The interdisciplinary collaboration is essential in understanding the life. The materials chemists can play a key role in the evolution of the nature.

4. Emerging applications

The potential applications of these materials in the traditional fields such as catalysis, separation, water purification and gas storage have been described in detail in a series of excellent review papers [52, 53]. In this part, only new emerging perspectives of applications in nanotechnology such as opto-electronics, biotechnology such as nanobiosensing and medical treatments such as controlled drug delivery will be illustrated by selected examples.

4.1. New phenomenon of ZnO nanoparticles in the channels of mesoporous silica CMI-1: quantum size effect and random laser effect

Among all the wide bandgap semiconductors studied up to now, zinc oxide ZnO is obviously the most interesting binary semiconductor (3.37 eV) [143] with very important optical properties which can be used in various fields such as short wavelength lasers, blue light emitting diodes, UV detectors, gas sensors, etc,… It is believed that ZnO with a large excitonic binding energy (60 meV), bio-safe and biocompatibility could be the next most important nanomaterials after carbon nanotubes. A recent and growing interest has been devoted to assemblies made of semiconductors incorporated in mesoporous materials. Such systems are often called nanocomposites. Different preparation techniques such as sol-gel [144, 145], impregnation [146, 147] and molecular capping [148, 149] have been used for the dispersion of ZnO particles in inorganic [144–147] or polymeric [148, 149] matrices. However, the aggregation of ZnO particles is unavoidable. The discovery of highly ordered mesoporous materials [4, 5] makes the control of nanoparticle size possible since the nanocrystallites are well confined into the pore system whose size is tunable by different methods. This should lead to potential applications in optoelectronics since size-dependent optical properties are expected as a result of quantum size effects (QSE).

The nanocomposite ZnO/mesoporous CMI-1 was prepared by the incipient wetness method [147] in a zinc nitrate aqueous solution. After drying, the powder was calcined at 550 °C in a flow of nitrogen for 12 h and then in flowing oxygen during 6 h.

The isotherm curves of both the starting CMI-1 and the obtained nanocomposite are type IV characteristic of mesoporous materials (*Fig. 1*). The mesoporosity of the material is thus maintained during the incorpora-

tion of ZnO. The pore size is rather homogenous as confirmed by the pore size distribution determined by the BJH [150] method. The morphology as well as the hexagonally channel arrays of nanocomposites remain unchanged during the incorporation of ZnO.

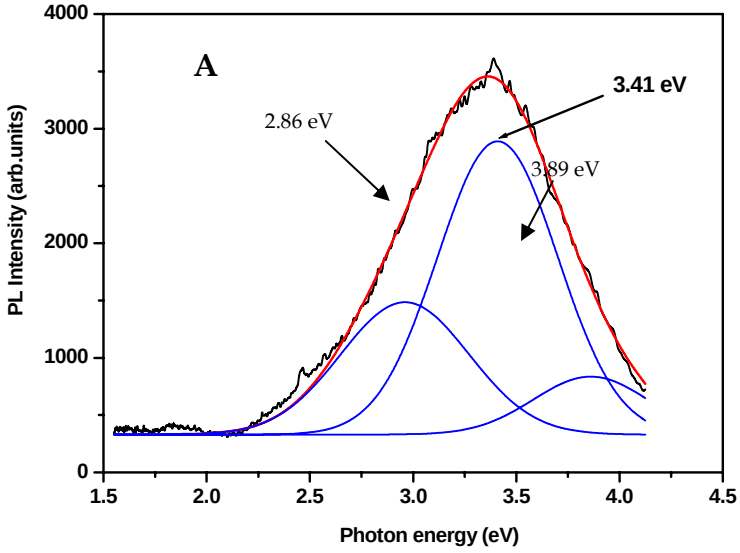

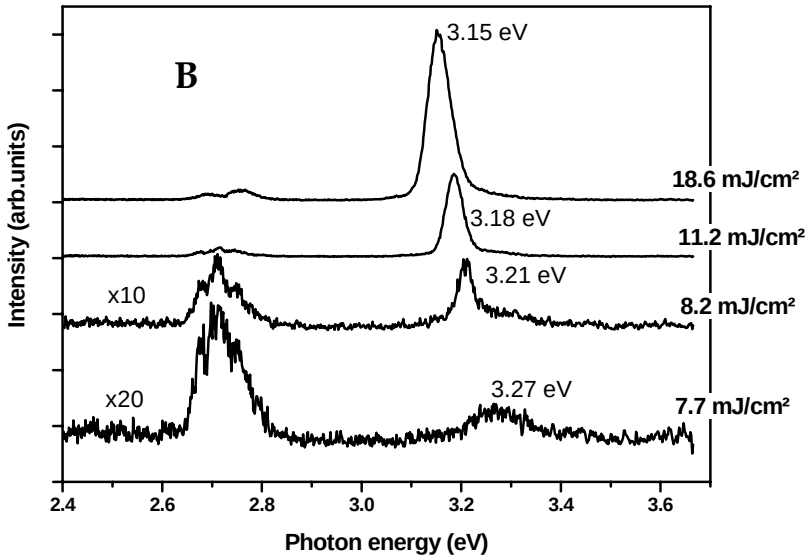

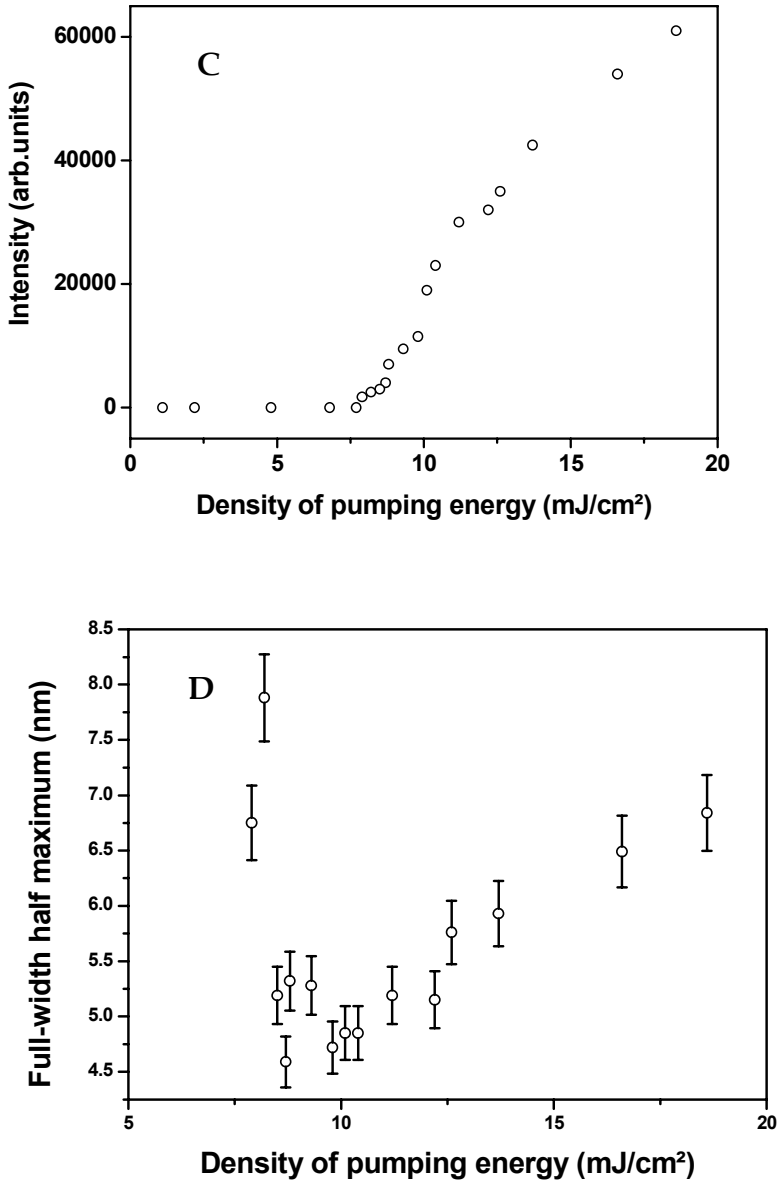

Fig. 16. (A) Photoluminescence spectrum (λ = 254 nm) of the ZnO-CMI-1 sample with its Gaussian decomposition; (B) Emission spectra (λ = 680 nm, E = 1.82 eV) of ZnO-CMI-1 sample for various pumping intensities; (C and D) Variation of the intensity (C) and of the FWHM (D) of the emission band of ZnO with the density of the pumping energy of the femtosecond laser (λ = 680 nm)

4.1.1. Optical properties

The photoluminescence band of ZnO particles is expected to be located at 3.28 eV [151] and comes from the excitonic recombination causing spontaneous emission. In our case, the PL spectroscopy gives a very wide PL band in the range 2.2–4.4 eV (*Fig. 16A*) which can be decomposed into three Gaussian peaks centred at 2.86, 3.41 and 3.91 eV, indicating three contributions. It is well known [152, 153] that the bands at 2.86 and 3.91 eV result from silica matrix. According to Sakurai [154], the band at 2.86 eV is caused by silinol groups and that at 3.89 eV is also stemmed from the defects of silica framework, only its real origin is not clear yet. The 3.41 eV PL band corresponds to the spontaneous emission of ZnO particles and is shifted to higher energies compared with that of bulk ZnO (3.28 eV). This shift is related to the QSE and is due to the small size of the ZnO nanoparticles. This QSE is quite important in opto-electronics. This study shows clearly that by using highly ordered mesoporous CMI-1, the particle size of ZnO can uniformly be tailored in the nanometrical range due to their unique pore structure.

4.1.2. Lasing effect

By submitting our samples to a 1.82 eV femtosecond laser excitation (which corresponds to a wavelength of 680 nm), we observed at low exciting intensities (7.7 mJ/cm^2) a broad emission band centred at 3.27 eV which is attributed to the spontaneous emission of the ZnO nanoparticles (*Fig. 16B*). When the pumping intensity reaches a threshold value (*ca.* 8.2 mJ/cm^2), the broad emission turns to a much narrower peak corresponding to stimulated emission. The threshold for the transition from spontaneous to stimulated emission can accurately be determined by studying the intensity variation and the full-width at half maximum (FWHM) of the band as a function of the energy delivered by the laser. According to both diagrams (*Fig. 16C* and *D*), the threshold value equals 8.2 mJ/cm^2 and represents the energy of the transition from spontaneous to stimulated emission from the nanoparticles of ZnO incorporated in the channels of the mesoporous CMI-1.

It is worth indicating that the photon energy used is not sufficiently high (1.82 eV) to excite one electron from the valence band to the conduction band of ZnO (gap = 3.37 eV). However, this phenomenon occurs indeed. This can only be produced by an excitation process implying two photons. The first photon sends one electron on a virtual level located in the bandgap (lifetime of around 10^{-16} s) and then the second photon excites the electron to the conduction band. Once the electron is excited, spontaneous

or stimulated emission can take place. The two-photon absorption occurs only if the time delay between the two photons is shorter than the lifetime of the electron on the virtual level. The two-photon absorption process is well known [155] but was never reported in ZnO nanoparticles grown in mesoporous materials. It is for the first time observed that the stimulated emission is produced after a two-photon absorption with ZnO (two-photon lasing effect). We believe that the stimulated emission occurs because the incident laser light scatters on ZnO nanoparticles loaded in the mesoporous material. If the laser light bounces from one particle to another and finally forms a loop, it can be trapped and amplified resulting in stimulated emission. This observation is quite promising in the conception of new laser sources for information storage.

4.2. A highly sensitive and selective fluorescence Nanobiosensor for Iron Ions: FI-DFO/Mesoporous silica CMI-1

The development of sensitive and selective fluorescent nanosensors for heavy and transition metal (HTM) ions has recently attracted much attention due to their importance in the fields of environmental monitoring, clinical toxicology, wastewater treatment and industrial processes. Towards the aim of creating a simple, stable and portable, cost-effective and long-lived nanobiosensor, designing and synthesising sensitive and selective HTM ions fluorosensor molecules and finding a suitable substrate for their immobilisation remain two significant challenges.

Here we illustrate as an example the first and important step towards the conception of highly sensitive and selective fluorescence nanobiosensors for iron ions. This was made by immobilisation within the channels of highly organized mesoporous silica CMI-1 of a bifunctional fluorophore molecule, Fluorescein-Desferrioxamine (FI-DFO), which combines the receptor of high selectivity for the complexing iron ions with analyst mediated signalling. The DFO has a very high complexation constant (log K) of 30.7 for Fe^{III} ions compared to Fe^{II} (7.2), Ni^{II} (10.9), Cu^{II} (14. 1), Zn^{II} (10.1) and Al^{III} (23.1) [156]. Fluorescein with a very high molar absorption coefficient of 63900 l/(mole.cm) is largely used in analytical chemistry as adsorption indicator for the titration of chloride ions with silver nitrate and is water soluble [157]. The complexation of DFO with Fe^{3+} ions induces the complete loss of the fluorescence of FI, called the fluorescence quenching. This example can be extended to prepare other highly efficient, selective and sensitive nano(bio)sensors.

The immobilisation of FI-DFO has firstly been performed by the impregnation method. However, the first testing has shown that the

prepared nanobiosensor has a strong leaching effect since the contact of nanobiosensor with Fe^{3+} ions in an aqueous solution leads to the release of a large quantity of FI-DFO immobilized in the mesochannels. This nanobiosensor cannot therefore be reused and regenerated. In order to create more favourable interactions (electrostatic, H-bonding and Van der Waals) between guest molecules and silicate matrices, internal surface of as-synthesized CMI-1 was modified with an aminopropyl-silane, before immobilisation of FI-DFO by impregnation. The new FI-DFO/surface functionalized CMI-1 nanobiosensor was characterized by TEM, SEM, XRD and N_2 adsorption techniques. No structural and morphological changes can be revealed after surface functionalisation and further immobilisation of FI-DFO by impregnation method. The initial typical morphology of CMI-1 material and highly organized mesochannels arrays remain unchanged. Only the pore volume, surface area and pore size appear decreased after surface functionalisation and a further decrease was noticeable after impregnation of FI-DFO, indicating the surface modification effect and the FI-DFO encapsulation. By spectrofluorimetry and compared with FI-DFO in liquid phase, a shift of 17 nm is observed and highlights a strong interaction between FI-DFO and CMI-1 mesoporous materials. This blue shift can be considered as a direct evidence of the real encapsulation of FI-DFO molecules within the materials, and their interaction with the aminopropyl grafted on the surface.

To evaluate the selectivity, efficiency and sensitivity to Fe^{3+} ions, the powders of the new FI-DFO/surface functionalized CMI-1 nanobiosensor (*Fig. 17A*) were pressed to thin wafers. An iron chloride solution was added dropwise onto the nanobiosensor wafer. The response of the nanobiosensor in presence of Iron ions was followed by spectrofluorimetry (*Fig. 17B*). A linear response of the nanobiosensor by increasing the FI-DFO/Fe^{3+} molar ratio was obtained (*Fig. 17C* and *D*). Our study showed the high selectivity and sensitivity of this nanobiosensor to Fe^{3+} ions. This is quite essential for a highly efficient sensor.

In summary, a highly efficient, selective and sensitive nanobiosensor for Fe^{3+} ions dosing has been developed by the encapsulation of the fluoresceine-desferrioxamine, a bifunctional fluoroionophore molecule, inside a highly ordered silica mesoporous material (*Fig. 17 A* and *B*). The method of encapsulation used is an impregnation technique which is very simple. The obtained nanobiosensor showed its high selectivity, sensitivity and efficiency (*Fig. 17 C* and *D*). The regeneration test is being carried out in our laboratory for a real clinical and environmental application. This example can have immediate impact on environmental monitoring, clinical toxicology, wastewater treatment and medical applications.

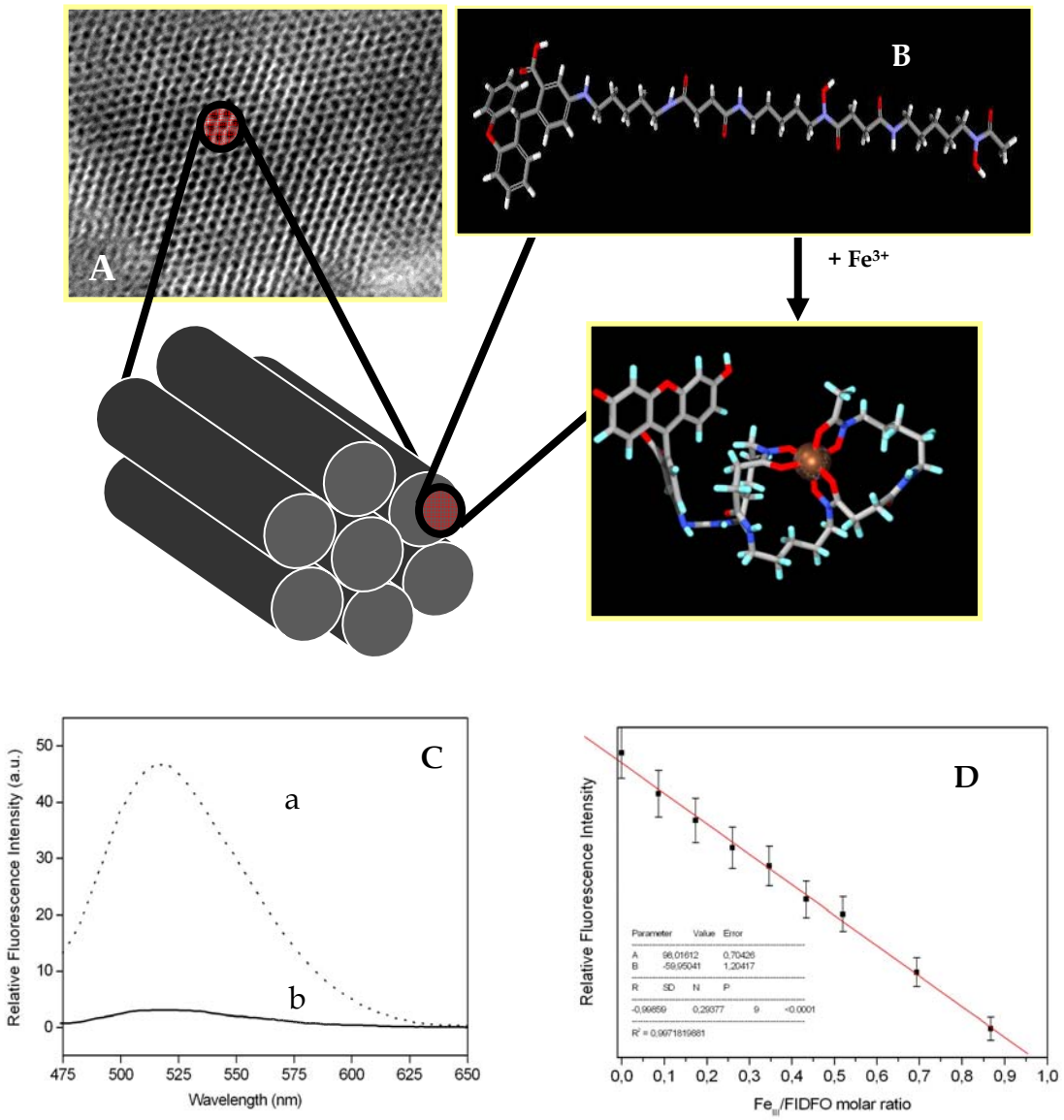

Fig. 17. (A) Immobilisation of FI-DFO in functionalized mesochannels of CMI-1; (B) FI-DFO molecules located in the mesochannels in free state with a extended conformation (a) and after complexation with Fe^{3+} ions (b); (C) Fluorescence test of FI-DFO in the absence (a) and presence (b) of Fe^{3+} ions; (D) A linear relationship of fluorescence of the conceived FI-DFO/functionalized CMI-1 nanobiosensor as a function of Fe^{3+} ions concentration in an aqueous solution

4.3. The highly structured mesoporous CMI-1 materials for the controlled drug delivery

The growth in biomedical knowledge leads to new research about new or existing bioactive molecules. As a consequence, the classical administration ways become inadequate for these high therapeutic potential molecules. Furthermore, these compounds are often unstable, poorly adsorbed, aqueous insoluble,… The great challenge is how to drive these molecules to their action sites.

Since 1980, significant advances have been made in the area of controlled drug release technology. The aim is to attempt to overcome drawbacks due to the use of conventional drugs and administration systems. Drug Delivery Systems (DDS) are able to modify the absorption and/or the distribution and/or the elimination of these drugs and then influence their pharmacokinetic profiles [158]. Thus, it is possible to maintain therapeutic drug levels for large periods of time to prevent the onset of potentially toxic peaks in drug concentration, to reduce the amount of drug and the number of administrations, and to protect the drug against chemical and enzymatic degradation [159].

Silica compounds seem to be suitable for such applications. In 1983, Unger proposed the utilisation of silica as new vector for drug delivery [160]. Biocompatible, the new silica vector does not generate any secondary effects for human body. The destruction of the silica matrix involves the hydrolysis of all siloxanes bindings. The $Si(OH)_4$ so formed is finally eliminated from human body by kidneys. Since this first experiment, several inorganic porous materials have been used including synthetic zeolites, silica xerogel materials and porous ceramic [161–164]. Among these materials, mesoporous molecular sieves attracted much attention from pharmaceutical industry and academia.

The immobiliszation of ibuprofen into the channels of our mesoporous material CMI-1 was performed in different solvents. Water was directly excluded because of the poor water-solubility of ibuprofen, only alcanes and ethanol were investigated. Best results were obtained with hexane and octane. Ethanol is very difficult to be eliminated from our charged material due to the formation of hydrogen bondings with the silanols of CMI-1, further preventing ibuprofen encapsulation. Using hexane or octane as immobilisation solvent, a very high drug charge rate of 30% can be obtained (*Fig. 18A*). The immobilisation of ibuprofen in hexane did not change the structural characteristics of material.

The *in vitro* release of ibuprofen has been performed in two simulated fluids: gastric fluid (HCl, pH = 1.2) for 30 minutes and then intestinal fluid

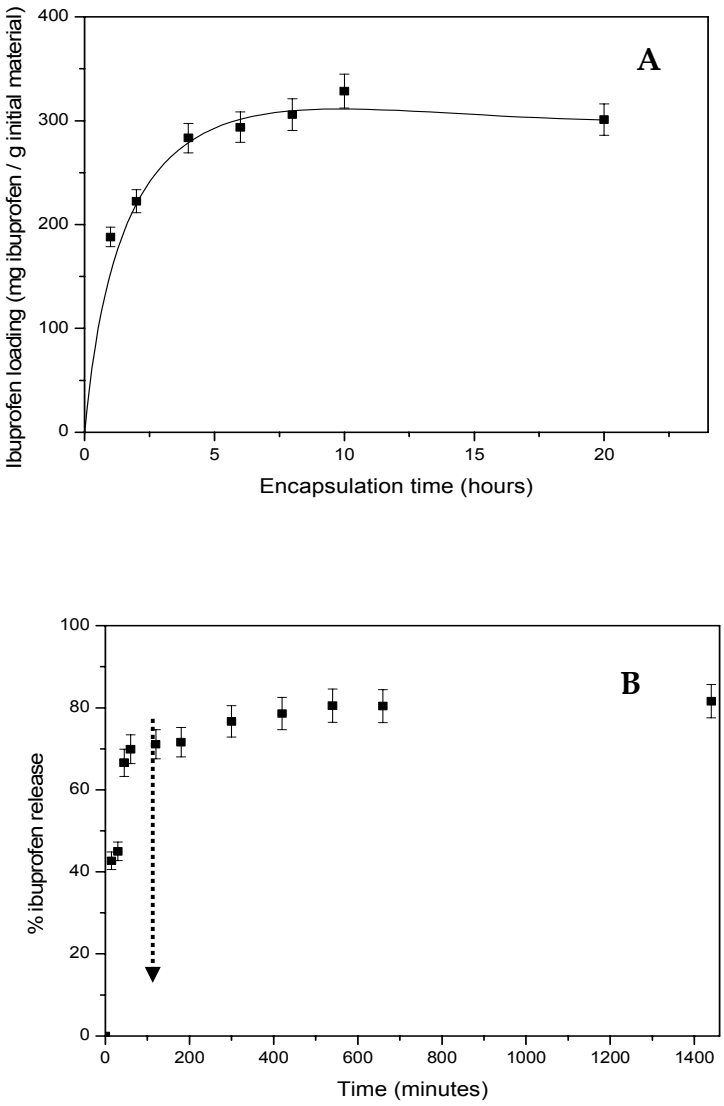

Fig. 18. (A) Ibuprofen loading as a function of encapsulation time (Initially CMI-1/ Ibuprofen ratio = 2/1) and (B) Ibuprofen release profile into gastric fluid during 30 minutes (pH = 1. 2) and then intestinal fluid (pH = 7. 4) and the arrow indicates the change from gastric fluid to intestinal fluid

(Na_3PO_4, NaOH, pH = 7.4) in order to simulate the behaviour of the material after oral administration (*Fig. 18B*). Ibuprofen (45%±5%) is released in the gastric fluid during the first 30 minutes. Then, after the passage to an intestinal fluid, the release can reach a plateau after 9 hours (80% ± 5%). This profile can be explained by solubility of ibuprofen at pH = 7.4. In fact, ibuprofen is almost insoluble in acid aqueous medium and reaches a solubility of 0.1 g ml^{-1} at pH = 7.4. So this better solubility at high pH values facilitates the transfer of drug molecules from the channels of CMI-1 to aqueous solution. This release profile is very promising for further pharmaceutical applications: the poorly water-soluble drug is protected from gastric medium and rapidly delivered in intestinal medium.

In summary, highly structured mesoporous CMI-1 materials constitute potentially interesting drug carriers for lipophilic drugs like ibuprofen. The mesoporous materials allow for the encapsulation of drug molecules inside its pores and to control the kinetic delivery of these molecules. The good stability of CMI-1 versus the gastric medium leads to a release of only 40% of the drug. While the drug release within intestinal medium can reach up to 80% of the drug initially included in CMI-1 mesopores, principally by a diffusion phenomenon: the molecule diffusion out of pores is very easy due to the size of the pores of the mesoporous material. Mesoporous CMI-1 presents a great interest for pharmaceutical application as Drug Delivery System, due to the unique properties of such materials.

5. General conclusions

We arrive at the end of this scientific trip in a very exciting, promising and extending field from mesoporous materials, meso-macroporous materials with a great variety in chemical compositions to some new and emerging applications in nanotechnology, biotechnology, medical applications and optoelectronics. Due to the limit of pages, it is not possible to describe all the aspects in a so huge and interdisciplinary domain which is being extended more and more. We just demonstrated in a very brief way some strategies for the conception of a series of mesoporous materials and hierarchically nanostructured meso-macroporous materials made in our laboratory (*Table 2*) and described in literature. For more details, two new review papers [45, 165] from our laboratory and a new review book with a series of young eminent authors can be useful [166]. Last point but not the least is that low dimensional nanostructures other than carbon nanotubes are another very attractive and promising domain [167–175] to which we pay also much attention despite non description in this paper.

Table 2. Description of a series of CMI materials

Materials	Description	Reference
CMI-1	Synthesized with $C_{16}(EO)_{10}$, TMOS, pH=2, *p6mm*	39, 42, 44, 45, 47, 48,
CMI-2	Synthesized with $C_{18}(EO)_{10}$, TMOS, pH=2, *p6mm*	43, 45, 50,
CMI-3	Synthesized with $C_{16}(EO)_{10}$, TMOS, pH=2 in the presence of metal ions such as Co^{2+}, Ni^{2+},…, *p6mm*	42, 45, 51
CMI-4	Synthesized with $C_{18}(EO)_{10}$, TMOS, pH=2 in the presence of metal ions such as Co^{2+}, Ni^{2+},…, *p6mm*	42, 45, 50,
CMI-5	Synthesized with CTMBA, Na silicate, pH=10 using alcanes as expanders, *hexagonal*	23–27, 45
CMI-6	Synthesized with CTMBA, Na silicate, pH=10 using alcanes+TMB expanders, *cubic*	23–27, 45
CMI-7	Meso-macroporous silicoaluminates, metal oxides, …	45, 99–105, 119, 120, 126–128, 140, 165, 176
CMI-8	Mesoporus carbon using CMI-1 silica as template	
CMI-9	Meso-macroporous carbons using CMI-7-Zr and CMI-7-SiAl as templates	

The self-formation strategy for hierarchically meso-macroporous materials [102, 120, 165, 176] will open exciting avenues for a new generation of functional materials with improved and tailorable properties for applications in various fields and has to be explored in depth. The immobilization of large biological cells within this kind of materials could allow us to design new bioreactors. This will also be a new important step for the combination of inorganic matrix and life torwards the creation of living materials. These materials have been applied in catalysis and have shown their superiority compared to traditional supports [177–181].

Acknowledgements

CB and NM thank the FNRS (Fonds National de la Recherche Scientifique, Belgium) for a FRIA fellowship. This work was realized in the frame of the Belgian Federal Government PAI-IUAP 01/5 project and was financially supported by the European Program of InterReg III (Programme France-Wallonie-Flandre, FW-2.1.5), the Wallonian Government (Gredecat, Convention n° 14574) and the FNRS (Convention n° 1.5.196.02F and 1.5.295.06).

References

1. A. Stein, *Adv. Mater.,* **15,** 763 (2003).
2. M. E. Davis, *Nature*, **417,** 813 (2002).
3. G. J. A. A. Soler-Illia, C. Sanchez, B. Lebeau, J. Patarin, *Chem. Rev.*, **102,** 4093 (2002).
4. C. T. Kresge, M. E. Leonowicz, W. J. Roth, J. C. Vartuli, J. S. Beck, *Nature*, **359,** 710 (1992).
5. J. S. Beck, J. C. Vartuli, W. J. Roth, M. E. Leonowicz, C. T. Kresge, K. D. Schmitt, C. T. W. Chu, D. H. Olsen, E. W. Sheppard, S. B. McCullen, J. B. Higgins, J. L. Schlenker, *J. Am. Chem. Soc.,* **114,** 10834 (1992).
6. D. Zhao, J. Feng, Q. Huo, N. Melosh, G. H. Fredrickson, B. F. Chmelka, G. D. Stucky, *Science*, **279,** 548 (1998).
7. D. Zhao, Q. Huo, J. Feng, B. F. Chmelka, G. D. Stucky, *J. Am. Chem. Soc.,* **120,** 6024 (1998).
8. B. T. Holland, C. F. Blanford, A. Stein, *Science*, **281**, 538 (1998).
9. C. F. Blanford, H. Yan, R. C. Schroden, M. Al-Daous, A. Stein, *Adv. Mater.,* **13,** 401 (2001).
10. H. W. Yan, C. F. Blanford, B. T. Holland, W. H. Smyrl, A. Stein, *Chem. Mater.,* **12**, 1134 (2000).
11. J. Fan, C. Yu, J. Lei, Q. Zhang, T. Li, B. Tu, W. Zhou, D. Zhao, *J. Am. Chem. Soc.,* **127**, 10794 (2005).
12. P. Yang, T. Deng, D. Zhao, P. Feng, D. Pine, B. F. Chmelka, G. M. Whitesides, G. D. Stucky, *Science*, **282,** 2244(1998).
13. R. Ryoo, S. H. Joo, S. J. Sun, *J. Phys. Chem. B,* **103,** 7743 (1999).
14. R. Ryoo, S. H. Joo, M. Kruk, M. Jaroniec, *Adv. Mater.,* **13**, 677 (2001).
15. S. Jun, S. H. Joo, R. Ryoo, M. Kruk, M. Jaroniec, Z. Liu, T. Ohsuna, O. Terasaki, *J. Am. Chem. Soc.,* **122,** 10712 (2000).
16. S. H. Joo, S. J. Choi, I. Oh, J. Kwak, Z. Liu, O. Terasaki, R. Ryoo, *Nature,* **412,** 9 (2001).
17. C. Vix-Guterl, S. Boulard, J. Parmentier, J. Werckmann, J. Patarin, *Chem. Lett.,* **10,** 1062 (2002).
18. C. N. R. Rao, A. Müller, A. K. Cheetham, *The Chemistry of Nanomaterials: Synthesis, Properties and Applications, Wiley-VCH, Weinheim* 1 (2004).
19. *Nanotechnology: Shaping the World Atom by Atom, National Science and Technology Council, Commitee on Technology, Washington D. C.* (1999).
20. A. F. Crønstedt, *Akad. Handl. Stockholm,* **17,** 20 (1756).
21. T. Linssen, K. Cassiers, P. Cool, E. F. Vansant, *Adv. Coll. Interf. Sci.,* **103,** 121 (2003).
22. J. L. Blin, C. Otjacques, G. Herrier, B. L. Su, *Intern. J. Inorg. Mater.*, **3,** 75 (2001).
23. J. L. Blin, G. Herrier, C. Otjacques, B. L. Su, *Stud. Surf. Sci. Catal.,* **128,** 57 (2000).
24. J. L. Blin, G. Herrier, C. Otjacques, B. L. Su, *Stud. Surf. Sci. Catal.,* **128,** 269 (2000).
25. J. L. Blin, G. Herrier, B. L. Su, *Stud. Surf. Sci. Catal.,* **129,** 75 (2000).
26. J. L. Blin, C. Otjacques, G. Herrier, B. L. Su, *Langmuir*, **16,** 4229 (2000).
27. J. L. Blin, B. L. Su, *Langmuir*, **18,** 5303 (2002).
28. Z. Y. Yuan, J. L. Blin, B. L. Su, *Chem. Commun.,* 504 (2002).
29. G. S. Attard, J. C. Glyde, C. G. Göltner, *Nature,* **378,** 366 (1995).
30. S. A. Bagshaw, E. Prouzet, T. J. Pinnavaia, *Science,* **269,** 1242 (1995).
31. S. A. Bagshaw, T. J. Pinnavaia, *Angew. Chem. Int. Ed. Engl.,* **10**, 1102 (1996).
32. P. T. Tanev, T. J. Pinnavaia, *Science,* **267,** 865 (1995).
33. E. Prouzet, T. J. Pinnavaia, *Angew. Chem. Int. Ed. Engl.,* **36,** 516 (1997).

34. E. Prouzet, F. Cot, G. Nabias, A. Larbot, P. Kooyman, T. J. Pinnavaia, *Chem. Mater*., **11,** 1498 (1999).
35. B. Lebeau, C. E. Fowler, S. Mann, C. Farcet, B. Charleux, C. Sanchez, *J. Mater. Chem.,* **10,** 2103 (2000).
36. C. Boissière, A. Larbot, E. Prouzet, *Chem. Mater*., **12,** 1937 (2000).
37. L. Sierra, J. L. Guth, *Microporous Mesoporous Mater.,* **27,** 243 (1999).
38. N. R. B. Coleman, G. S. Attard, *Microporous Mesoporous Mater.,* **44–45,** 73 (2001).
39. J. L. Blin, A. Léonard, B. L. Su, *J. Phys. Chem. B,* **105,** 6070 (2001).
40. J. L. Blin, G. Herrier, B. L. Su, *Stud. Surf. Sci. Catal*., **129,** 67 (2000).
41. J. L. Blin, A. Leonard, G. Herrier, G. Philippin, B. L. Su, *Stud. Surf. Sci. Catal.,* **141,** 117 (2002).
42. J. L. Blin, A. Léonard, B. L. Su, *Chem. Mater.,* **13,** 3542 (2001).
43. G. Herrier, J. L. Blin, B. L. Su, *Langmuir,* **17,** 4422 (2001).
44. J. L. Blin, A. Becue, B. Pauwels, G. Van Tendeloo, B. L. Su, *Microporous Mesoporous Mater.,* **44–45,** 41 (2001).
45. B. L. Su, A. Leonard, Z. Y. Yuan, *C. R. Chimie*, **8,** 713 (2005).
46. D. J. Mitchell, G. J. T. Tiddy, L. Waring, T. Bostock, M. P. McDonald, *J. Chem. Soc. Faraday Trans., I,* **79**, 975 (1983).
47. A. Léonard, J. L. Blin, M. Robert, P. A. Jacobs, A. K. Cheetham, B. L. Su, *Langmuir,* **19,** 5484 (2003).
48. A. Léonard, J. L. Blin, P. A. Jacobs, P. Grange, B. L. Su, *Microporous Mesoporous Mater.,* **63,** 59 (2003).
49. W. Zhang, B. Glomski, T. R. Pauly, T. J. Pinnavaia, *Chem. Commun.,* 1803 (1999).
50. G. Herrier, B. L. Su, *Stud. Suf. Sci. Catal.,* **135,** 1305 (2001).
51. A. Léonard, J. L. Blin, G. Herrier, B. L. Su, *Stud. Suf. Sci. Catal.,* **146,** 243 (2003).
52. A. Corma, *Chem. Rev.,* **97,** 2373 (1997).
53. A. Corma, A. Martinez, V. Martinez-Soria, J. B. Monton, *J. Catal.,* **153,** 25 (1995).
54. A. Corma, M. S. Grande, V. Gonzalez-Alfaro, A.V. Orchilles, *J. Catal.,* **159,** 375 (1996).
55. M. Selvaraj, A. Pandurangan, K. S. Seshadri, P. K. Sinha, V. Krishnasamy, K. B. Lal, *J. Mol. Catal. A : Chem.,* **186,** 173 (2002).
56. Q. N. Le, R. T. Thomson, *U. S. Patent 5,232,580* (1993).
57. A. Sakthivel, S. K. Badamali and P. Selvam, *Microporous Mesoporous Mater.,* **39,** 457 (2000).
58. A. Armengol, M. L. Cano, A. Corma, H. Garcia, M. T. Navarro, *Chem. Commun.,* 519 (1995).
59. M. P. Coles and R. F. Jordan, *J. Am. Chem. Soc.,* **119,** 8125 (1997).
60. D. T. On, D. Desplantier-Giscard, C. Danumah, S. Kaliaguine, *Appl. Catal. A: Gen*., **53,** 545 (2003).
61. A. Léonard, N. Moniotte, B. L. Su, (2006) *to be published.*
62. A. Léonard, J. L. Blin, B. L. Su, *Coll. Surf. A: Phys. Eng. Asp.,* **241,** 87 (2004).
63. A. Léonard, B. L. Su, (2006) *to be published.*
64. V. Parvulescu, C. Dascalescu, B. L. Su, *Stud. Surf. Sci. Catal*., **135**, 4772 (2001).
65. V. Parvulescu, B. L. Su *Catal. Today*, **69**, 315 (2001).
66. V. Parvulescu, C. Anastasescu, Ch. Constantin, B. L. Su, *Stud. Surf. Sci Catal.,* **142,** 1204 (2002).
67. V. Parvulescu, B. L. Su, *Stud. Surf. Sci. Catal*., **142**, 1403 (2002).
68. Ch. Constantinescu, V. Parvulescu, A. Dobre, A. Bujor, G. Popescu, B. L. Su, *Stud. Surf. Sci. Catal*., **143,** 67 (2002).

69. V. Parvulescu, B. L. Su, *Stud. Surf. Sci. Catal.,* **143,** 575 (2002).
70. V. Parvulescu, C. Anastasescu, B. L. Su, *J. Mol. Catal. A. Chem.*, **198,** 249 (2003).
71. V. Parvulescu, C. Anastasescu, C. Constantin, B. L. Su, *Catal. Today,* **78,** 477 (2003).
72. V. Parvulescu, C. Dascalescu, B. L. Su, *Stud. Surf. Sci. Catal.*, **146,** 629 (2003).
73. V. Parvulescu, C. Constantin, B. L. Su, *J. Mol. Catal. A. Chem.*, **202**, 171 (2003).
74. V. Parvulescu, C. Anastasescu, B. L. Su, *J. Mol. Catal. A. Chem.*, **198, 2**49 (2003).
75. C. Constantin, V. Parvulescu, A. Bujor, G. Popescu, B. L. Su, *J. Mol. Catal. A. Chem.*, **208,** 245 (2004).
76. V. Parvulescu, C. Constantin, G. Popescu, B. L. Su, *J. Mol. Catal. A. Chem.*, **208,** 253 (2004).
77. V. Parvulescu, C. Anastasescu, B. L. Su, *J. Mol. Catal. A. Chem.*, **211,** 143 (2004).
78. V. Parvulescu, B. L. Su, *Catal. Today*, **93–95,** 307 (2004).
79. V. Parvulescu, E. Sacaliuc, C. Anastasescu,B. L. Su, *Stud. Surf. Sci. Catal.*, **154,** 2603 (2004).
80. M. Shibagaki, K. Tabakahashi, H. Matsushita, *Bull. Chem. Soc. Jpn.,* **61,** 3283 (1988).
81. T. Yokoyama, T. Setoyama, N. Fujita, M. Nakajima, T. Maki, *Appl. Catal. A. Gen.,* **4,** 149 (1992).
82. J. A. Knowles, M. J. Hudson, *Chem. Commun*., 2083 (1995).
83. A. Kim, P. Bruinsma , Y. Chen, L. Q. Wang, J. Liu, *Chem. Commun.,* 161 (1997).
84. G. Pacheco, E. Zhao, A. Garcia, A. Sklyarov, J. J. Fripiat, *Chem. Commun.,* 491 (1997).
85. P. Yang, E. Zhao, D. I. Margolese, B. F. Chmelka, G. D. Stucky, *Chem. Mater.,* **11,** 2813 **(**1999**).**
86. J. L. Blin, L. Gigot, A. Léonard, B. L. Su, *Stud. Surf. Sci. Catal.,* **141,** 257 (2002).
87. J. L. Blin, A. Léonard, L. Gigot, O. Provost, B. L. Su, *Stud. Surf. Sci. Catal.,* **146,** 443 (2003).
88. J. L. Blin, L. Gigot, A. Léonard, B. L. Su, *Stud. Surf. Sci. Catal.,* **143,** 1053 (2002).
89. J. L. Blin, R. Flamant, B. L. Su, *Intern. J. Inorg. Mater.*, **3,** 959 (2001).
90. T. Z. Ren, Z. Y. Yuan, B. L. Su, *Chem. Phys. Lett.*, **374,** 170 (2003).
91. Z. Y. Yuan, B. L. Su, *Chem. Phys. Lett.*, **381**, 710 (2003).
92. M. Kruk, M. Jaroniec, R. Ryoo, S. H. Joo, *J. Phys. Chem. B.,* **104,** 7960 (2000).
93. S. H. Joo, S. Jun, R. Ryoo, *Microporous Mesoporous Mater.,* **44–45,** 153 (2001).
94. S. S. Kim, T. J. Pinnavaia, *Chem. Commun.,* 2418 (2001).
95. J. Lee, S. Yoon, S. M. Oh, S. Shin, T. Hyeon *Adv. Mater.,* **12** 1359 (2000).
96. S. Alvarez, A. B. Fuertes, *Carbon,* **42,** 433 (2004).
97. M. O. Coppens, J. H. Sun, T. Maschmeyer, *Catal. Today,* **69,** 331 (2001).
98. J. H. Sun, Z. Shan, T. Maschmeyer, M. O. Coppens, *Langmuir,* **19,** 8395 (2003).
99. Z. Y. Yuan, T. Z. Ren, B. L. Su, *Adv. Mater.*, **15,** 1462 (2003).
100. T. Z. Ren, Z. Y. Yuan, B. L. Su, *Langmuir*, **20,** 1531 (2004).
101. T. Z. Ren, Z. Y. Yuan, B. L. Su, *Chem. Phys. Lett.*, **388,** 46 (2004).
102. T. Z. Ren, Z. Y. Yuan, B. L. Su, *Chem. Commun*., 2730 (2004).
103. Z. Y. Yuan, T. Z. Ren, A. Azioune, J. J. Pireaux, B. L. Su, *Catal. Today*, **105,** 647 (2005).
104. Z. Y. Yuan, T. Z. Ren, B. L. Su, *Chem. Phys. Lett.*, **383,** 348 (2004).
105. T. Z. Ren, Z. Y. Yuan, B. L. Su, *Colloid. Surf. A. Phys. Eng. Asp.,* **241,** 67 (2004).
106. G. de la Puente, E. Falabella Sousan-Aguiar, A. Figueiredo-Costa, U. Sedran, *Appl. Catal. A: Gen.,* **242,** 381 (2003).

107. W. Deng, M. W. Toepke, B. H. Shanks, *Adv. Funct. Mater.,* **13,** 61 (2003).
108. A. Imhof, D. J. Pine, *Nature,* **389,** 948 (1997).
109. O. D. Velev, T. A. Jede, R. F. Lobo, A. M. Lenhoff, *Nature,* **389,** 447 (1997).
110. B. Lebeau, C. E. Fowler, S. Mann, C. Farcet, B. Charleux, C. Sanchez, *J. Mater. Chem.*, **10,** 2105 (2000).
111. D. M. Antonelli, *Microporous Mesoporous Mater.,* **33,** 209 (1999).
112. A. Caruso, M. Antonietti, *Adv. Funct. Mater.,* **12,** 307 (2002).
113. M. Antonietti, B. Berton, C. Göltner, H. P. Hentze, *Adv. Mater.,* **10,** 154 (1998).
114. D. Zhao, P. Yang, B. F. Chmelka, G. D. Stucky, *Chem. Mater.*, **11,** 1174 (1999).
115. S. A. Davis, S. L. Burkett, N. H. Mendelson, S. Mann, *Nature,* **385,** 420 (1997).
116. K. Nakanishi, *J. Porous Mater.,* **4,** 67 (1997).
117. J. Sun, Z. Shan, T. Maschmeyer, *Chem. Commun.,* 2670 (2001).
118. A. Hui, F. Schüth, *C. R. Chimie,* **8,** 609 (2005).
119. A. Léonard, J. L. Blin, B. L. Su, *Chem. Commun.,* 2568 (2003).
120. A. Léonard, B. L. Su, *Chem. Commun.,* 1674 (2004).
121. A. Collins, D. Carriazo, S. A. Davis, S. Mann, *Chem. Commun.*, 568 (2004).
122. Y. Amenomiya, *Appl. Catal.,* **30,** 57 (1987).
123. K. D. Dobson, A. J. McQuillan, *Langmuir,* **13,** 3392 (1997).
124. L. Shi, K. C. Tin, N. B. Wong, *J. Mater., Sci.,* **34,** 3367 (1999).
125. E. M. Logothetis, *Chem. Sensor Technol.,* **3,** 89 (1991).
126. J. L. Blin, A. Léonard, L. Gigot, Z. Y. Yuan, A. Vantomme, A. K. Cheetham, B. L. Su, *Angew. Chem. Int. Ed.,* **42,** 2872 (2003).
127. Z. Y. Yuan, A. Vantomme, A. Léonard, B. L. Su, *Chem. Commun.,* 1558 (2003).
128. A. Vantomme, Z. Y. Yuan, B. L. Su, *New J. Chem.,* **28,** 1083 (2004).
129. D. M. Antonelli, J. Y. Ying, *Angew. Chem. Int. Ed.,* **34,** 2014 (1995).
130. V. F. Stone, R. J. Davis, *Chem. Mater.*, **10,** 1468 (1998).
131. D. T. On, *Langmuir,* **15,** 8561 (1999).
132. S. Cabrera, J. El-Haskouri, A. Beltran-Porter, D. Beltran-Porter, D. D. Marcos, P. Amoros, *Solid State Sci.*, **2,** 513 (2000).
133. P. Yang, D. Zhao, D. I. Margolese, B. F. Chmelka, G. D. Stucky, *Nature,* **395,** 583 (1998).
134. L. Wang, S. Tomura, M. Maeda, F. Ohashi, K. Inukai, M. Suzuki, *Chem. Lett.,* 1414 (2000).
135. X. Wang, J. C. Yu, C. Ho, X. Fen, *Langmuir,* **21,** 2552 (2005).
136. K. Tanabe, *Catalysis Today,* **78,** 68 (2003).
137. O. Unal, M. Akinc., *J. Am. Ceram. Soc.,* **78,** 805 (1996).
138. D. J. Iiett, M. Saiful Islam, *J. Chem. Soc. Faraday Trans.,* **891,** 3833 (1993).
139. G. A. M. Hussein, B. C. Gates, *J. Catal.*, **176,** 395 (1998).
140. Z. Y. Yuan, T. Z. Ren, B. L. Su, *Chem. Mater.*, **10,** 5096 (2004).
141. S. Mann, *Chem. Commun.*, 1 (2004).
142. J. Aizenberg, J. C. Weaver, M. S. Thanawala, V. C. Sunder, D. E. Morse, P. Fratzl, *Science*, **309,** 275 (2005).
143. C. Klingshirn, *Phys. Stat. Sol.* B, **71,** 547 (1975).
144. C. Cannas, C. Casu, A. Musinu, A. Lai, G. Piccaluga, *J. Mater. Chem.*, **9,** 1765 (1999).
145. S. Lu, L. Zhang, X. Yao, *Chin. Sci. Bull.,* **41,** 1923 (1996**).**
146. W. H. Zhang, J. L. Shi, L. Z. Wang, D. S. Yan, *Chem. Mater.,* **12,** 1408 (2000).
147. S. E. Dapurkar, S. K. Badamali, P. Selvam, *Catal. Today*, **68,** 63 (2001).

148. M. Oner, J. Norwig, W. H. Meyer, G. Wegner, *Chem. Mater.*, **10,** 460 (1998).
149. L. Guo, S. Yang, C. Yang, P. Yu, J. Wang, W. Ge, *Chem. Mater.*, **12,** 2268 (2000**).**
150. E. P. Barret, L. G. Joyner, P. P. Halenda, *J. Am. Chem. Soc.*, **73,** 373 (1951).
151. I. Ozerov, D. Nelson, A. V. Bulgakov, W. Marine, M. Sentis, *Appl. Surf. Sci.*, **212,** 349 (2003).
152. J. H. Stathis, M. A. Kastner, *Phys. Rev. B*, **35,** 2972 (1987).
153. L. N. Skuja, A. N. Streletsky, A. B. Pakovich, *Solid State Commun*., **50,** 1069 (1984).
154. Y. Sakurai, *J. Non-Crystal. Solids*, **271,** 218 (2000).
155. Y. D. Glinka, S. H. Lin, Y. T. Chen, *Phys. Rev. B*, **62,** 4733 (2000).
156. H. Keberle, *Ann. N. Y. Acad. Sci.*, **119,** 758 (1964).
157. A. F. Rodde, *J. Phys. Chem.*, **72,** 756 (1968).
158. R. Langer, *Nature*, **392,** 5 (1998).
159. D. D. Breimer, *Adv. Drug Deliv. Rev.*, **33,** 265 (1998).
160. K. Unger, H. Rupprecht, B. Valentin, W. Kircher, *Drug Develop. Ind. l Pharm.*, **9,** 69 (1983).
161. P. Kortesuo, M. Ahola, M. Kangas, I. Kangasniemi, A. Yli-Urpo, J. Kiesvaara, *Internl. J. Pharm.*, **200,** 223 (2000).
162. M. Ahola, P. Kortesuo, I. Kangasniemi, J. Kiesvaara, A. Yli-Urpo, *Internl. J. Pharm.*, **195,** 219 (2000).
163. V. Ambrogi, G. Fardella, G. Grandolini, L. Perioli, *Intern. J. Pharm.*, **220,** 23 (2001).
164. C. Uglea, I. Albu, A. Vatajuna, M. Croitoru, S. Antoniu, L. Panaitescu, R. Otttenbrite, *J. Biomater. Sci. Polymer Ed.*, **6**, 633 (1994).
165. Z. Y. Yuan, B. L. Su, *J. Mater. Chem.*, **16,** 663 (2006).
166. G. Q. Lu, S. X. Zhao, *Nanoporous Materials, Science and Engineering*, Imperial College Press, Singapore, 2004.
167. Z. Y. Yuan, B. L. Su, *Chem. Commun*., 1202 (2002).
168. Z. Y. Yuan, J. F. Colomer, B. L. Su, *Chem. Phys. Lett*., **363,** 362 (2002).
169. Z. Y. Yuan, Z. Zhang, G. Duand, T. Z. Ren, B. L. Su, *Chem. Phys. Lett*., **378,** 349 (2003).
170. Z. Y. Yuan, X. Zhang, B. L. Su, *Appl. Phys. A*, **78,** 1063 (2004).
171. Z. Y. Yuan, B. L. Su, *Chem. Phys. Lett.*, **389,** 83 (2004).
172. Z. Y. Yuan, B. L. Su, *Colloids Surf. A,* **241,** 173 (2004).
173. Z. Y. Yuan, T. Z. Ren, B. L. Su, *Appl. Phys. A*, **80,** 743 (2005).
174. F. Xu, Z.Y. Yuan, G. H. Du, T. Z. Ren, C. Bouvy, M. Halasa, B. L. Su, *Nanotechnology*, **17**, 588 (2006).
175. C. Bouvy, W. Marine, R. Sporken, B.-L. Su, *Chem. Phys. Lett*., **420**, 225 (2006).
176. Z. Y. Yuan, T. Z. Ren, A. Azioune, J. J. Pireaux and B. L. Su, *Chem. Mater.*, **18**, 1753 (2006).
177. V. Idakiev, L. Ilieva, D. Andreeva, J. L. Blin, L. Gigot, B. L. Su, *Appl. Catal. A. Gen*., **243,** 25 (2003).
178. V. Idakiev, T. Tabakova, Z. Y. Yuan, B. L. Su, *Appl. Catal. A. Gen.*, **270**, 135 (2004).
179. V. Idakiev, Z. Y. Yuan, B. L. Su, *Appl. Catal. A. Gen.*, **281**, 149 (2005).
180. L. Ilieva, J. W. Sobczak, M. Manzoli, B. L. Su, D. Andreeva, *Appl. Catal. A. Gen*., **291**, 85 (2005).
181. V. Idakiev, T. Tabakova, A. Naydenov, Z. Y. Yuan, B. L. Su, *Appl. Catal. B. Environ*., **63**, 178 (2006)